A&A 443, 251–269 (2005)
DOI: 10.1051/0004-6361:20053294

Astronomy & Astrophysics

Structural parameters of the hot pulsating B subdwarf Feige 48 from asteroseismology⋆,⋆⋆

S. Charpinet[1], G. Fontaine[2], P. Brassard[2], M. Billères[3], E. M. Green[4], and P. Chayer[5,6]

[1] UMR 5572, Université Paul Sabatier et CNRS, Observatoire Midi-Pyrénées, 14 Av. E. Belin, 31400 Toulouse, France
e-mail: scharpin@ast.obs-mip.fr
[2] Département de Physique, Université de Montréal, C.P. 6128, Succursale Centre-Ville, Montréal QC, H3C 3J7, Canada
e-mail: [fontaine;brassard]@astro.umontreal.ca
[3] European Southern Observatory, Santiago Headquarters, Av. A. de Cordova 3107, Vitacura, Casilla 19001, Santiago 19, Chile
e-mail: mbillere@eso.org
[4] Steward Observatory, University of Arizona, 933 North Cherry Avenue, Tucson, AZ 85721, USA
e-mail: bgreen@as.arizona.edu
[5] Department of Physics and Astronomy, Johns Hopkins University, 3400 North Charles Street, Baltimore, MD 21218-2686, USA
e-mail: chayer@pha.jhu.edu
[6] Primary affiliation: Department of Physics and Astronomy, University of Victoria, PO Box 3055, Victoria, BC V8W 3P6, Canada

Received 25 April 2005 / Accepted 21 July 2005

ABSTRACT

We present observations followed by a thorough analysis of the rapidly pulsating subdwarf B star (or EC 14026 star) Feige 48. This work is part of a long term multifaceted effort to exploit the strong asteroseismological potential of sdB pulsators which involves high sensitivity photometric observations, accurate spectroscopic measurements, and the development of appropriate modelling tools dedicated to the interpretation of the seismic data. Our model atmosphere analysis of the time averaged optical spectrum of Feige 48 obtained at the new Multiple Mirror Telescope (MMT) leads to estimates of $T_{\rm eff} = 29\,580 \pm 370$ K and $\log g = 5.480 \pm 0.046$ (with $\log N({\rm He})/N({\rm H}) = -2.95 \pm 0.08$), in excellent agreement with previous spectroscopic measurements of its atmospheric parameters. This places Feige 48 close to the red edge of the EC 14026 instability region in the $\log g - T_{\rm eff}$ plane. A standard Fourier analysis of our high signal-to-noise ratio Canada-France-Hawaii Telescope (CFHT) light curves reveals the presence of nine distinct harmonic oscillations with periods in the range 343−383 s, a significant improvement over previous reported observations that recovered only five periods (Koen et al. 1998, MNRAS, 300, 1105; Reed et al. 2004, MNRAS, 348, 1164). Out of these nine periods, only four turn out to be independent modes having different k and/or ℓ indices suitable for detailed asteroseismology. The remaining periods can be interpreted as rotationally split components of modes with the same (k, ℓ) values, but different m indices that bear the signature of the rotation of the star. On the basis of the four independent periods, we have carried out a detailed asteroseismic analysis of Feige 48 using the well-known forward method. Our analysis leads objectively to the identification of the (k, ℓ) indices of the four independent periods identified in the star, and to the determination of its structural parameters. The periods correspond to low-order modes with adjacent values of k and with $\ell = 0$, 1, and 2. They define a band of unstable modes, in agreement with nonadiabatic pulsation theory. Furthermore, the average dispersion between the observed periods and the periods of the corresponding theoretical modes of the optimal model is only ∼0.005%, quite close to the actual accuracy of the observations. We emphasise that radiative levitation is a key ingredient in the determination of accurate pulsation periods for sdB stars, and that standard models with uniform metallicity fail to reproduce the observed periods in Feige 48 because they do not incorporate this key piece of constitutive physics. On the basis of our combined spectroscopic and asteroseismic analysis, the inferred global structural parameters of Feige 48 are $T_{\rm eff} = 29\,580 \pm 370$ K, $\log g = 5.4365 \pm 0.0060$, $\log M_{\rm env}/M_* = -2.97 \pm 0.09$, $M_* = 0.460 \pm 0.008\ M_\odot$ (i.e., close to the canonical mass of extreme horizontal branch stars), $R/R_\odot = 0.2147 \pm 0.0034$, and $L/L_\odot = 31.62 \pm 2.58$. Combined with detailed model atmosphere calculations, we estimate, in addition, that this star has an absolute visual magnitude $M_V = 3.961 \pm 0.062$ and is located at a distance $d = 794 \pm 30$ pc (using $V = 13.46 \pm 0.02$). Finally, the analysis of the fine structure indicate a rotation period of $P = 9.44 \pm 1.18$ h, leading to an equatorial velocity of $V_{\rm eq} = 27.6 \pm 3.9$ km s^{-1}. With a $V_{\rm eq} \sin i \lesssim 5$ km s^{-1} limit set by Heber et al. (2000, A&A, 363, 198), this result means that Feige 48 is a moderate rotator which, with an inclination angle $i \lesssim 10.4 \pm 1.7°$, is seen nearly pole-on.

Key words. stars: interiors – stars: oscillations – stars: subdwarfs – stars: individual: Feige 48

⋆ Based on photometric observations gathered at the Canada-France-Hawaii Telescope, operated by the National Research Council of Canada, the Centre National de la Recherche Scientifique of France, and the University of Hawaii. Spectroscopic observations reported here were obtained at the MMT Observatory, a joint facility of the University of Arizona and the Smithsonian Institution.

⋆⋆ This study made extensive use of the computing facilities offered by the Calcul en Midi-Pyrénées (CALMIP) project, France.

1. Introduction

In the grand scheme of the evolution of stars, hot subdwarf B (sdB) stars are commonly seen as objects that populate the so-called Extreme Horizontal Branch (EHB; Heber 1986; Saffer et al. 1994). These correspond to low-mass ($\sim$0.5 $M_{\odot}$) He-core burning stars with an extremely thin ($\lesssim$0.02 $M_{\odot}$), mostly inert hydrogen rich residual envelope which evolve directly toward the white dwarf cooling sequence after core helium exhaustion, thus bypassing the Asymptotic Giant Branch (AGB) and Planetary Nebulae (PN) evolutionary stages (Dorman et al. 1993). If the fate of hot B subdwarfs is relatively well understood within this evolutionary framework, how such stars happen to be formed remains, however, one of the unsolved questions. Various scenarios have been proposed over the years to address this problem, involving either single star evolution with enhanced mass loss at the tip of the Red Giant Branch (D'Cruz et al. 1996), or binary evolution following various concurrent channels from common envelope ejection, stable Roche lobe overflow, to the merger of two helium white dwarfs (see, e.g., Han et al. 2002, 2003, and references therein). Interestingly, the latter scenarios would lead to a somewhat broader dispersion of stellar masses among sdB stars (between 0.30–0.70 $M_{\odot}$) than is currently assumed from canonical EHB models.

The recent discoveries of both rapid and slow multiperiodic nonradial oscillations in a fraction of the field sdB stars is therefore of particular interest in the current context. The rapid sdB pulsators known as the *V361 Hya* stars, but more commonly referred to as the EC 14026 stars, were the first to be observationally detected by colleagues from the South African Astronomical Observatory (SAAO; Kilkenny et al. 1997). At that same epoch, the existence of this class of pulsators was also predicted by Charpinet et al. (1996) in an independent theoretical effort aimed at identifying potential mechanisms that could destabilise pulsation modes in EHB models. This prediction emerged from the discovery that an efficient opacity (κ–)mechanism associated with the accumulation of iron due to microscopic diffusion processes is at work in the envelopes of sdB stars. Charpinet et al. (1997) confirmed that, indeed, remarkable similarities exist between appropriate EHB pulsation models (i.e., the so-called "second generation" models which take diffusion of iron into account) and the most basic properties of EC 14026 pulsators (see also the review of Charpinet et al. 2001). Various surveys by the SAAO group, by the Montréal group (see Billères et al. 2002), by a Norwegian-German-Italian team (see, e.g., Silvotti et al. 2002), and by other teams (see the reviews of Charpinet 2001 and Kilkenny 2002) rapidly led to additional discoveries, bringing the total of known EC 14026 pulsators to 33 at the time of writing. The EC 14026 stars tend to cluster at high effective temperatures and surface gravities (near $T_{\rm eff} \sim 33\,500$ K and $\log g \sim 5.8$), although outliers indicate a relatively large dispersion of these stars in the $\log g - T_{\rm eff}$ diagram. The periods detected in EC 14026 stars typically range from $\sim$100 s to $\sim$200 s, but can be substantially longer for class members having lower surface gravities (e.g., 290–600 s for PG 1605+072; see Charpinet 2001, and reference therein). Their mode amplitudes usually span a relatively wide range, but typical values are of several millimagnitudes. In most cases, the short periods are entirely consistent with low-order, low-degree radial and nonradial acoustic waves (Charpinet et al. 1997, 2001; Stobie et al. 1997). In low surface gravity sdB pulsators, however, the presence in the observed period spectrum of low-order g-modes or mixed modes cannot be excluded and may somewhat complicate the identification of the true nature of the modes being detected (Charpinet et al. 2002a).

Green et al. (2003) recently established that B subdwarfs also host a second, seemingly independent class of multiperiodic pulsators showing significantly longer periods. These long period sdB variables (the so-called PG 1716+426, but sometimes also referred to as the "Betsy" stars or the "lpsdBV" stars) populate the low-temperature/low-gravity corner ($T_{\rm eff} \lesssim 30\,000$ K, $\log g \lesssim 5.7$) of the region in the $\log g - T_{\rm eff}$ plane where sdB stars are found. Their multiperiodic luminosity variations occur on typical timescales of $\sim$45 min to $\sim$2 h (i.e., much longer than the periods observed in the EC 14026 stars), implying that relatively high-order gravity modes are involved. Remarkably, the same mechanism responsible for the oscillations in the EC 14026 stars is thought to operate in the long period sdB pulsators as well, but destabilising this time high-order, $\ell \gtrsim 3$ gravity modes (Fontaine et al. 2003).

The existence of these two distinct classes of pulsators among the hot B subdwarfs is of particular interest since p-modes and g-modes probe different regions of their interiors (see Charpinet et al. 2000). One can therefore envision to collect complementary information on EHB stars in general from the study of these two classes of pulsators. While it is too early to assess the real asteroseismological potential of the newly discovered PG 1716+426 stars, the EC 14026 pulsators have already proved to be excellent laboratories for asteroseismic studies. In the pioneering work of Brassard et al. (2001), the acquisition of high signal-to-noise ratio data at the Canada-France-Hawaii 3.6 m Telescope (CFHT) combined with efforts to develop a new global optimisation method for asteroseismology led to the first successful attempt to match *simultaneously all* the detected periods of the short period sdB pulsator PG 0014+067. This also led to the first asteroseismological determination of the fundamental parameters of a sdB star. Further improvements at the level of our global optimisation technique along with dedicated high-sensitivity CFHT photometry yielded similar outcomes for a few other rapid sdB pulsators, as illustrated by the results of Charpinet et al. (2003) on the star PG 1047+003 and, most recently, by the thorough analysis of the star PG 1219+534 described in Charpinet et al. (2005). Each of these studies have emphasised the importance of obtaining asteroseismological solutions that accurately reproduce the pulsation periods and which, at the same time, are entirely consistent with both the surface parameters ($T_{\rm eff}$ and $\log g$) derived from independent quantitative spectroscopy, and with the prediction of the nonadiabatic pulsation calculations obtained using the "second generation" models of Charpinet et al. (1997, 2001). Such a consistency between three independent aspects of the modelling of these stars – namely, period distribution calculations, model atmosphere computations, and nonadiabatic mode stability predictions – certainly adds to the credibility of these asteroseismological results.

In this paper, we present the detailed asteroseismic analysis of the short-period pulsating sdB star Feige 48 (V* KL UMa). Koen et al. (1998) were the first to report on short period nonradial oscillations in that star, revealing a relatively simple spectrum of 5 periods found in the range 344−379 s (see also Reed et al. 2004), i.e., somewhat longer than in most of the other known EC 14026 stars. Estimated surface parameters from quantitative spectroscopy provided by these authors indicate that Feige 48 is among the coolest known rapid sdB pulsators, which places it close to the red edge of the instability domain (Charpinet et al. 2001). Interestingly, O'Toole et al. (2004) have recently established that Feige 48 is also the member of a relatively close binary system with an orbital period of ∼9.02 h. The unseen companion is likely a white dwarf, although the hypothesis of a cool main sequence star could not be completely ruled out.

Our analysis is based on additional, high signal-to-noise ratio white light photometry obtained at the CFHT which leads us to almost double the number of detected periods in Feige 48. This significant improvement at the level of the photometry, added to new improved spectroscopy made on that star, permitted the application of our global optimisation technique, leading ultimately to the determination of its fundamental parameters. In the following sections, we fully report on our combined photometric and spectroscopic observations of Feige 48 (Sect. 2) and discuss the detailed analysis of the photometric light curve obtained for that star (Sect. 3). Then, we present the outcome of the detailed asteroseismic analysis we have carried out on Feige 48 based on these new observations (Sect. 4). A summary and conclusions uprising from this analysis are then provided in Sect. 5.

2. Observations

2.1. Medium resolution spectroscopy

Feige 48 was first classified as a "faint blue star" by Feige (1958) and was eventually recognised as a sdB star by Graham (1970). More recent Strömgren photometry from Wesemael et al. (1992) gives $y = 13.456$, $(b-y) = -0.116$, $(u-b) = -0.162$, and $m_1 = 0.086$, indicative of a relatively bright and apparently isolated hot B subdwarf (which it is not, however, according to O'Toole et al. 2004).

Spectroscopic estimates for the surface parameters of Feige 48 were first proposed in the paper of Koen et al. (1998). These authors obtained a spectrum of that star with the intermediate-dispersion spectrograph of the 2.5 m Isaac Newton Telescope which was then analysed using a Balmer line profile fitting procedure based on profiles computed from LTE grids of model atmospheres, as described in Saffer et al. (1994). Note that these authors used grids with zero helium abundance, as no He I line was visible in their spectrum. From their analysis, Koen et al. (1998) have derived $T_{\rm eff} = 28\,900 \pm 300$ K and $\log g = 5.45 \pm 0.05$ for the atmospheric parameters of Feige 48.

Heber et al. (2000) analysed a Keck HIRES spectrum of Feige 48 using line blanketed NLTE and LTE model atmospheres to derive atmospheric parameters, metal abundances, and a limit on the projected rotational velocity of that star. In the conclusion of their detailed comparative study, they adopted as their best values $T_{\rm eff} = 29\,500 \pm 300$ K, $\log g = 5.50 \pm 0.05$, and $\log N({\rm He})/N({\rm H}) = -2.93 \pm 0.05$, which is in agreement with the previous Koen et al. (1998) measurement. The very sharp metal lines seen in the Keck HIRES spectrum also allowed Heber et al. (2000) to constrain the projected rotational velocity of Feige 48 by setting a limit of $V \sin i \lesssim 5$ km s^{-1} (see also O'Toole et al. 2004), indicating, at this stage, that this star is either a relatively slow rotator, an object seen nearly pole-on, or both.

In order to double check on the spectroscopy of the star Feige 48, we obtained additional measurements from which we derived independent estimates for its atmospheric parameters. A medium resolution (∼1 Å), high S/N ratio (∼203 per pixel, with 3.1 pixels per resolution element) spectrum of that star was obtained recently with the blue spectrograph at the new 6.5 m Multiple Mirror Telescope (MMT). Another observation, a low-resolution (∼8.7 Å), high S/N ratio (∼249 per pixel, with 2.6 pixels per resolution element) spectrum, was also gathered at the Steward Observatory 2.3 m telescope. Such observations are part of a global program aimed at improving the spectroscopic characterisation of sdB stars, and in particular of EC 14026 pulsators and long period sdB pulsators (the PG 1716+426 stars). A simultaneous fit of the available Balmer lines (Hβ to Hδ for the medium-resolution spectrum and Hβ to H9 for the low-resolution spectrum) and neutral helium lines within a grid of profiles from our recent NLTE H/He model atmospheres was performed (see Charpinet et al. 2005 for details). As in the case of PG 1219+534 discussed by these authors, both solutions agree within the measurement errors. We show the resulting fit to our MMT spectrum in Fig. 1, with uncertainties given on the parameters corresponding to the formal errors of the fit. More realistic estimates of the uncertainties were obtained by comparing the results of fitting similar spectra gathered over different nights (see Green, Fontaine, & Chayer, in preparation), and from this we conservatively adopted the values of $T_{\rm eff} = 29\,580 \pm 370$ K, $\log g = 5.480 \pm 0.046$, and $\log N({\rm He})/N({\rm H}) = -2.95 \pm 0.08$ as our best estimates for the atmospheric parameters of Feige 48. We point out that these values are remarkably consistent with those derived independently by Koen et al. (1998) and Heber et al. (2000).

2.2. Time series photometry

We observed Feige 48 in optical "white light" fast photometric mode at the Canada-France-Hawaii 3.6 m Telescope (CFHT) during a six-night run scheduled on 1998, June. Table 1 provides a journal of these observations. As with our previous programs, the photometric data were gathered with LAPOUNE, the portable Montréal three-channel photometer. The data were then carefully corrected for various undesirable effects (e.g., atmospheric transparency variations, extinction, etc.) using the data reduction package OSCAR specifically designed by one of us (P.B.) for that purpose. We refer the interested reader to Billères et al. (1997) for details on the observations and data reduction procedures.

Table 1. CFHT high time resolution photometric observations of Feige 48.

Run number	Date (UT)	Start time (UT)	Sampling time (s)	Total number of data points	Resolution (mHz)
cfh-064	1998-06-26	06:00	10	1014	0.099
cfh-066	1998-06-27	05:53	10	992	0.101
cfh-069	1998-06-28	05:51	10	986	0.101
cfh-073	1998-06-29	05:51	10	1000	0.100
cfh-076	1998-06-30	05:50	10	998	0.100
cfh-079	1998-07-01	06:43	10	660	0.152

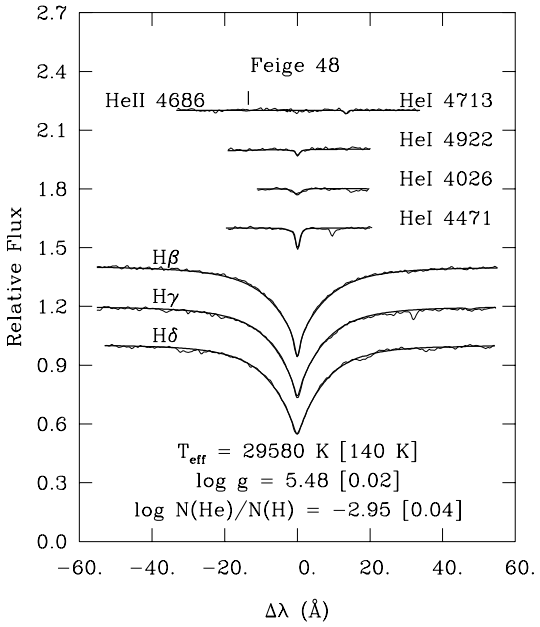

Fig. 1. Model fit (solid curve) to the Hβ, Hγ, and Hδ hydrogen Balmer lines and neutral helium lines available in our time averaged high S/N medium-resolution optical spectrum of Feige 48. Note the presence of a few metal lines and the fact that the He II 4686 line is absent in this relatively cool EC 14026 pulsator.

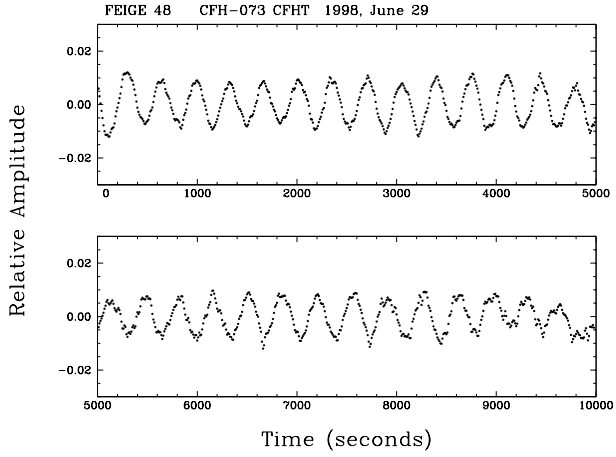

Fig. 2. Representative optical light curve obtained on Feige 48 during the night of 1998, June 29. Each band covers an interval of 5000 s and the amplitude is expressed in terms of the residual intensity relative to the mean brightness of the star. Each plotted point represents a sampling time of 10 s.

The observing conditions were excellent throughout most of the run, allowing us to acquire six consecutive high signal-to-noise ratio time series of about three hours each on Feige 48. This leads to a frequency resolution in the Fourier domain of 2.17 μHz for a relatively modest duty cycle of 12.8%, quite sufficient, however, to extract pulsation periodicities in that star (see below). Obtaining longer light curves each night would have been possible, but the plans were to share the available observing time with two other sdB pulsators of high interest (namely KPD 2109+4401 and PG 0014+067). The quality of the data gathered during these observations is illustrated in Fig. 2 which displays a representative light curve obtained on 1998, June 29 (run cfh-073). The brightness modulation detected in Feige 48 has a typical peak-to-peak amplitude of less than ∼3% and is dominated by a pseudo-period of ∼350 s. Figure 2 strongly suggests, however, that other periodicities are involved in the variations. The multiperiodic nature of the variations is confirmed in the Fourier amplitude spectrum shown in Fig. 3 and the detailed analysis of the light curve (see below) reveals that, indeed, at least as many as nine periodicities contribute to the luminosity variations seen in Feige 48.

3. Analysis of the light curve

We analysed the complete time series of Feige 48 in a standard manner by combining Fourier analysis, least-squares fits to the light curve, and prewhitening techniques. The procedure to extract pulsation modes from the light curve is now greatly eased by a new dedicated software named BERTHE, developed recently by one of us (P.B.). This software provides powerful tools to conveniently apply the procedure described, for instance, in Charpinet et al. (2005). Nine frequencies (periods) could be extracted from our time series of Feige 48. The prewhitening sequence is first illustrated globally with the successive Fourier transforms shown in Fig. 3 (from *top* to *bottom*). The upper curve represents the full amplitude spectrum in the 0−8 mHz frequency bandpass where photometric activity has been detected. We note that in the domain extending from 8 mHz up to the Nyquist frequency (50 mHz, as we used a sampling time of 10 s), the structures found in the Fourier amplitude spectrum are entirely consistent with noise. At the low frequency end, the rms noise level increases due to residual atmospheric variations (which are difficult to remove completely) and no obvious periodicities were found. All

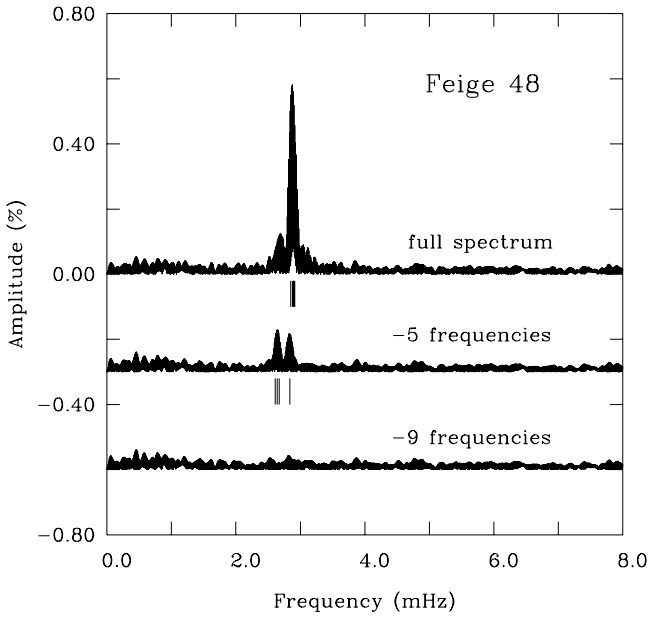

Fig. 3. Fourier amplitude spectrum and residuals after prewhitening of the identified periods (frequencies) in the time series.

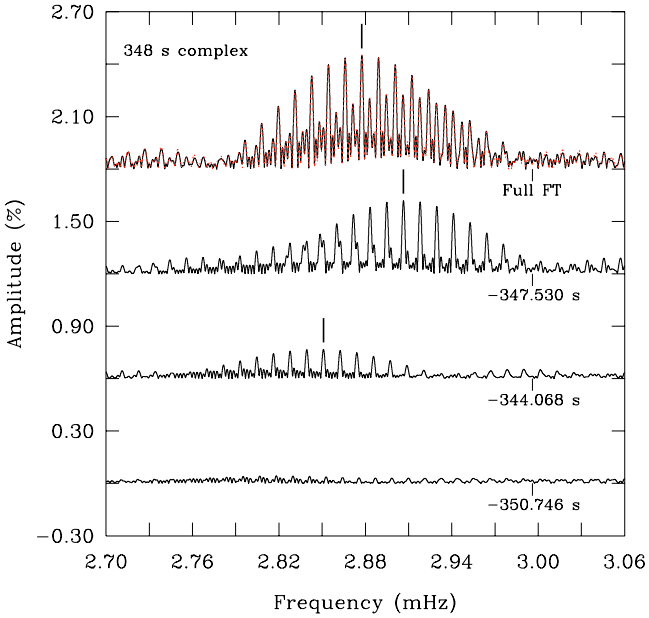

Fig. 4. Close-up view of the prewhitening sequence of the 348 s mode complex. From top to bottom, successive curves show the Fourier amplitude spectrum after prewhitening of the identified period and its associated window pattern. The red dotted curve superimposed to the full Fourier spectrum (top curve) is the spectrum reconstructed on the basis of the extracted harmonic oscillations.

significant power appears to be concentrated in a narrow band covering the range 2.5−3.0 mHz. The middle curve in Fig. 3 shows the Fourier transform of the residual light curve after prewhitening of five of the dominant harmonic oscillations. This leads to the detection of four additional frequencies that clearly emerge above the detection threshold (set, as is standard, to 3.7 times the rms noise level, estimated at ∼0.01% locally). The lower curve displays the Fourier transform of the residual light curve after prewhitening of all nine identified periodicities, indicating that no significant power is left.

Close-up views of the prewhitening sequences that led to the detection of the nine periodicities are shown in Figs. 4–6. Fourier transforms of time series with a relatively poor coverage like those used in this study may suffer from severe aliasing of the real frequencies and one must deal with the inherent difficulty of choosing the right peaks among the available structures. In particular, due to interference patterns and the presence of noise, a peak corresponding to a real frequency (as opposed to aliases of this frequency) may not necessarily be the one with the highest amplitude in the Fourier space. Consequently, our approach was to experiment with various combinations of peak selections, keeping ultimately the one that leads to the "flattest" residual (bad selections that include aliases usually produce remaining structures in the residual). For stars with a relatively simple pulsation spectrum, such as Feige 48, this procedure ensures with a reasonable level of confidence that the true periodicities are indeed recovered. The intricate structures seen at the scale of Figs. 4–6, which are made of real frequencies plus their associated daily aliases (separated by 11.57 μHz), can clearly be decomposed in multiple components. For instance, the 348 s complex illustrated in Fig. 4 shows structures that can be decomposed, through prewhitening, in three components of an almost perfectly symmetric triplet. Since no power is left in the residual, this is a clear indication that the real frequencies have been picked up and

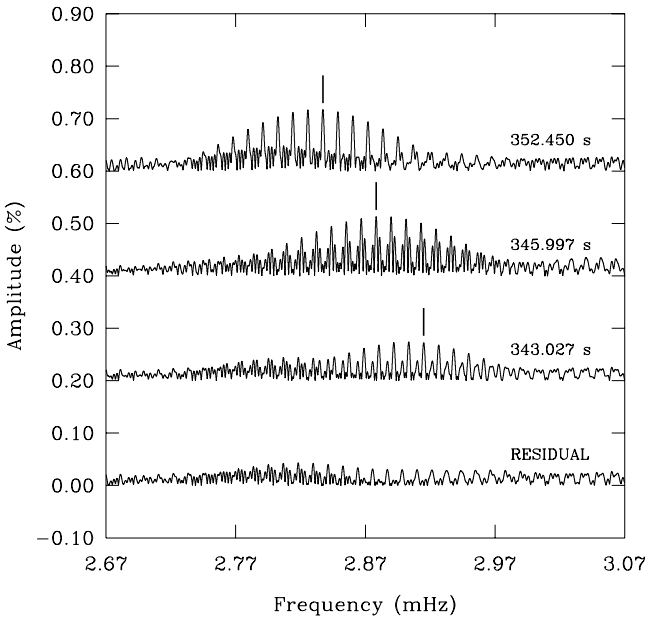

Fig. 5. Close-up view of the prewhitening sequence of the 352 s mode complex. From top to bottom, successive curves show the Fourier amplitude spectrum after prewhitening of the identified period and its associated window pattern.

the associated oscillations removed correctly from the pulsation signal present in the light curve. Similarly, we could extract the six additional periodicities as shown in Figs. 5 and 6, leading to "flat" residuals with no obvious periodicity left above the mean noise level.

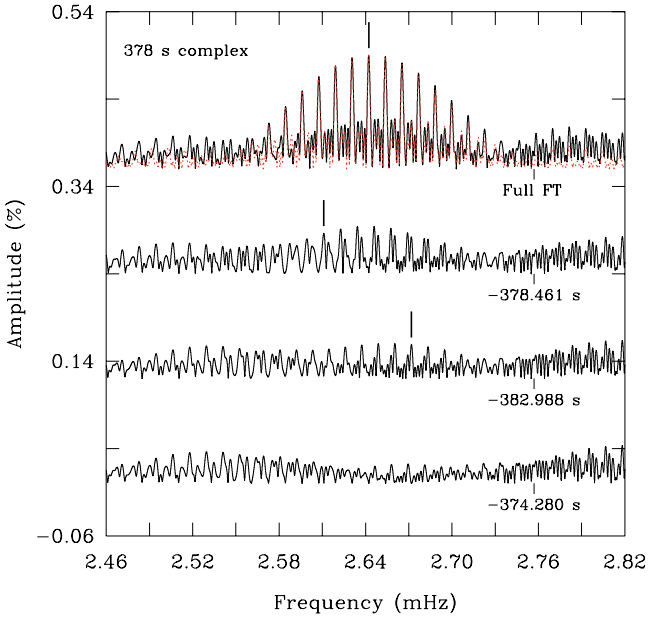

Fig. 6. Close-up view of the prewhitening sequence of the 378 s mode complex. *From top to bottom*, successive curves show the Fourier amplitude spectrum after prewhitening of the identified period and its associated window pattern. The red dotted curve superimposed to the full Fourier spectrum (*top curve*) is the spectrum reconstructed on the basis of the extracted harmonic oscillations.

Table 2. Harmonic oscillations detected in the light curve of Feige 48.

ID	Frequency (mHz)	Period (s)	Amplitude (%)	Spacing (μHz)	Reed et al. (2004) Period (s)
f_1^+	2.91522	343.027	0.071	+25.0	...
f_1	2.89020	345.997	0.111	...	(346.01)
f_2^+	2.90640	344.068	0.411	+28.9	344.08
f_2	2.87745	347.530	0.640	...	347.56
f_2^-	2.85107	350.746	0.165	−26.4	350.75
f_3	2.83728	352.450	0.116	...	352.40
f_4^+	2.67180	374.280	0.039	+29.5	...
f_4	2.64228	378.461	0.131	...	378.50
f_4^-	2.61105	382.988	0.043	−31.2	...

We provide in Table 2 a list of the detailed properties that characterise the nine harmonic oscillations uncovered. These are the frequency (in mHz), the period (in seconds), the amplitude (in % of the mean brightness), and the frequency spacing between multiplet components (in μHz). In addition to the results of our frequency analysis based on the 15.6 h of CFHT data acquired, we also mention the results of the extensive analysis of Reed et al. (2004) which was based on more than 380 h of low S/N ratio photometry collected on Feige 48 over a period of five years with small telescopes. Their analysis led to the firm identification of five periodicities with some hints for a couple more. Those five periodicities correspond to the five periods already discovered by Koen et al. (1998). In comparison, our CFHT light curves allowed us to recover with no ambiguity not only those five pulsation modes but four additional ones. This significant improvement in the number of modes detected – a crucial step for the purpose of asteroseismology – is of course a direct consequence of the much higher sensitivity of the data gathered at the CFHT and underlines one more time, if need be, the importance of high S/N ratio observations in the asteroseismological process. As a last check of the reliability of our detailed Fourier analysis, Fig. 7 represents, in the relevant 2.0−4.0 mHz frequency bandwidth, the full Fourier transform of the observed light curve of Feige 48 and the Fourier transform of the noiseless light curve reconstructed on the basis of the nine harmonic oscillations listed in Table 2 (shown upside down). The point-by-point difference in the frequency domain between these two curves leaves a residual (shown shifted downward in the figure) that provides a quantitative measure of how well the observations are reproduced in the Fourier space. An examination of the Fourier spectrum, the model spectrum, and their residual indicates that the light curve is satisfactorily reproduced on the basis of the parameters given in Table 2 along with the phases that have been measured. We note that the residual is quite flat, as would be expected for a successful reconstruction.

One can construct four separate groups of modes from the nine periods uncovered: two triplets referred to as (f_2^-, f_2, f_2^+) and (f_4^-, f_4, f_4^+) in Table 2, a doublet (f_1, f_1^+), and a singlet (f_3). It is then noticeable that, in each group (except, of course, for the singlet), all the modes are evenly distributed in frequency with a mean spacing of $\overline{\Delta\nu} \sim 28.2\,\mu$Hz. Such symmetric structures are usually caused by the slow rotation of the star that lifts the degeneracy in frequency of pulsation modes with the same ℓ and k indices, but different m values. This interpretation of the fine structure in the frequency spectrum of Feige 48 and its implications will be discussed further in Sect. 4.6. The presence of several multiplets indicates that, however, not all periods among the nine uncovered will be useful for the asteroseismic analysis. In terms of seismic constraints placed on the stellar structure, modes that constitute, in the period spectrum, the fine structure caused by rotational splitting (i.e., modes with the same k and ℓ indices, but different values of m) do not bring additional information. Only the central ($m = 0$) component carries information about the global structure of the star. The frequencies of the $m \neq 0$ components relative to the central component are essentially determined by the rotation rate. Assuming solid rotation, the frequencies of the m components are, to first order, $\nu_{k\ell m} = \nu_{k\ell 0} - m(1 - C_{k\ell})/P_{\rm rot}$, where $P_{\rm rot}$ is the rotation period of the star. The first-order rotation coefficient $C_{k\ell}$ does depend on stellar structure, but it is numerically much smaller than unity for the p-modes seen in sdB pulsators ($C_{k\ell} < 0.02$, in most cases) and it can be neglected in a first approximation. Thus, for p-modes, $\nu_{k\ell m} \simeq \nu_{k\ell 0} - m/P_{\rm rot}$, showing no additional model dependency (which is all contained in the frequency $\nu_{k\ell 0}$ of the central component) other than the rotation rate of the star. In other words, in terms of asteroseismic constraints on the fundamental stellar parameters, a multiplet must be seen as a *single* mode, and only periods of *independent* modes (i.e., with different values of ℓ and/or k) are relevant for the asteroseismology of EC 14026 stars. For Feige 48, we are thus left with only four independent modes – namely f_1, f_2, f_3, and f_4 – to do the asteroseismology. With such a small

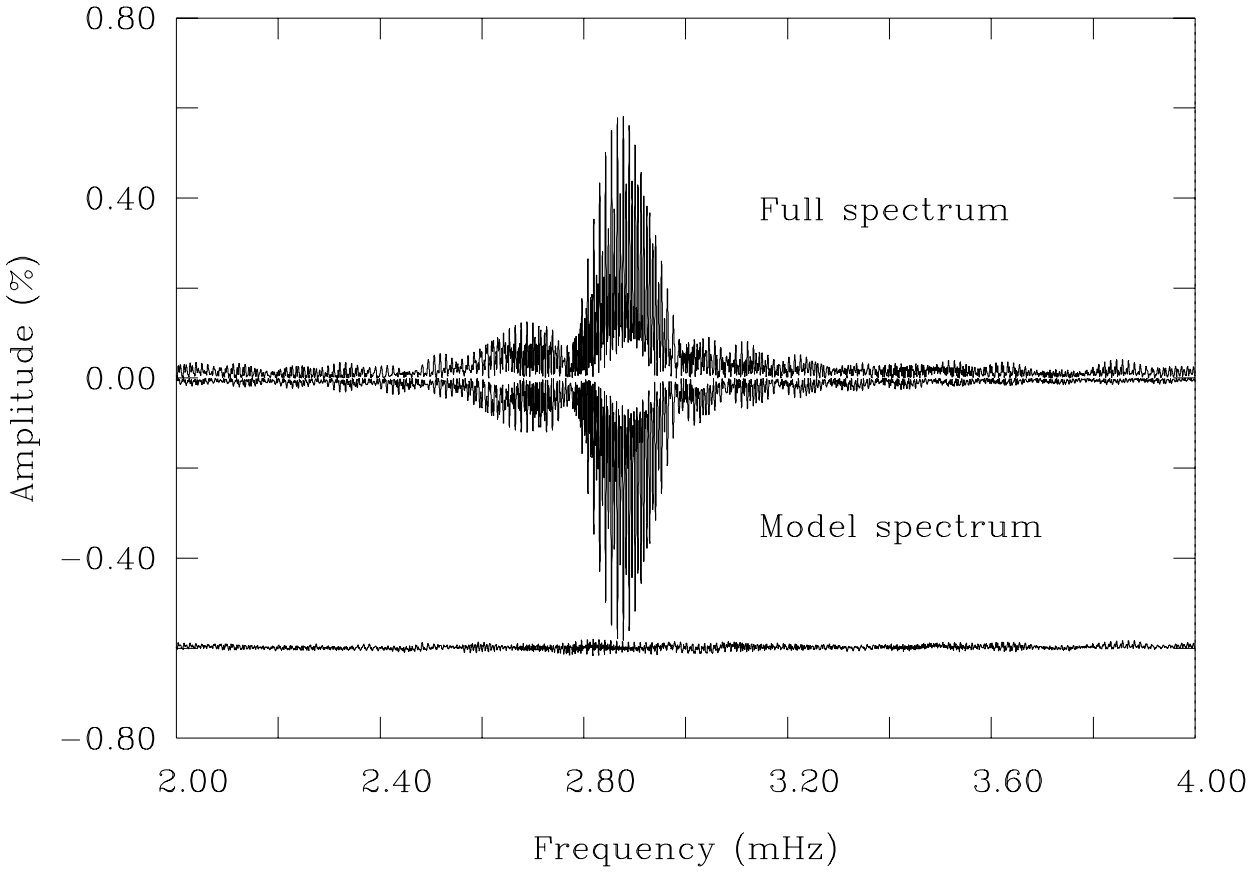

Fig. 7. *Upper half*: Fourier amplitude spectrum of the complete light curve of Feige 48 in the 2–4 mHz bandwidth. *Lower half*: Fourier amplitude spectrum (plotted upside down) of the noiseless light curve reconstructed on the basis of the 9 harmonic oscillations listed in Table 2. In addition, the point-by-point frequency difference between the "observed" Fourier spectrum and the "computed" spectrum is shown, but shifted downward by 0.60%.

number of independent periods, the analysis of this star may appear somewhat compromised due to the lack of seismic constraints. Fortunately, it turns out that the additional constraints brought about by accurate spectroscopic measurements are sufficient to allow for the extraction of useful seismic information on this star.

4. Asteroseismic interpretation

4.1. Models and method

The asteroseismological interpretation of the period spectrum of pulsating stars has often been impaired by the lack of identification of the modes being observed. The analysis of EC 14026 stars is confronted by similar challenges as white light fast photometry generally gives little clue on the degree ℓ and/or radial order k of the modes detected. For Feige 48, we dispose of no a priori knowledge of the geometry of the nine observed modes. Some hints on the degree ℓ of these modes exist, however, since fine structure, most likely due to rotation, has been detected in the period spectrum. Such hints, although not sufficient to uniquely identify the modes, may be used as additional constraints in the search for models that can best-match the observed periods.

We have applied to Feige 48 the new global optimisation method that we have developed in the past few years. Our approach, described in some detail in Charpinet et al. (2005), is based on the well known forward method which consists of comparing directly periods computed from stellar models to periods observed in the star under consideration with the goal of reproducing as accurately as possible its oscillation spectrum. Applied to EC 14026 stars, it requires a double-optimisation procedure that takes place simultaneously at the period matching level and in the model parameter space. The first optimisation is aimed at finding the combination (or mode identification) that leads to the best possible *simultaneous* match of *all* the observed periods to the periods computed for a given model. The quality of the fit is evaluated through a quantity, $\overline{\chi}^2$, derived from a least-squares formalism. In the present case, we implemented the information contained in the fine structure of the period spectrum into the period matching procedure as an additional constraint based on the "$2\ell+1$ splitting rule", i.e., we assumed, for instance, that triplets can only be nonradial modes of degree $\ell = 1$ or more, but cannot be radial ($\ell = 0$) modes. We also carried out computations without making use of such constraints. The second optimisation consists of localising the optimal model (or models) that minimises the "merit" function, $\overline{\chi}^2(a_1,a_2,...,a_N)$, in the N-dimensional model parameter space (considering the general case), leading

objectively to the best period match of the observations. For the analysis of Feige 48, we used the Toulouse package of numerical tools specifically developed for such objective asteroseismic studies. It includes a genetic algorithm based period matching code that performs the first optimisation part, a parallel grid computing code useful to explore the parameter space and visualise the complex shape of the $\overline{\chi}^2$ function, and a parallel multimodal genetic algorithm based optimisation code designed to explore efficiently the vast N-dimensional parameter space and seek for the optimal solutions. We recall that this approach is built on the very basic requirement that models pretending to provide a good asteroseismological fit of the spectrum of a pulsating star *must* match *all* the observed periods *simultaneously*, i.e., the procedure is a *global* optimisation. Moreover, we stress that the solutions identified from this approach do not rely on any previous mode identification. The mode identification appears instead naturally as the solution of the global fitting procedure, i.e., the mode identification obtained is the one that provides the best *simultaneous* match of *all* the detected periods.

Application of our double-optimisation scheme to EC 14026 stars requires computing appropriate theoretical period spectra that need to be compared with the observed periods. Three codes are involved in this process, starting with an equilibrium model building code first described in Brassard & Fontaine (1994) and adapted to produce the so-called "second generation" models suitable for pulsating sdB stars (see Charpinet et al. 1997, 2001, 2005). In particular, these static models are superior to all evolutionary structures currently available in that they incorporate the nonuniform iron abundance profiles predicted by the theory of microscopic diffusion assuming an equilibrium between gravitational settling and radiative levitation. Diffusion leads to the constitution of a reservoir of iron in the H-rich envelope of subdwarf B stars with significant iron enrichments produced locally which are responsible, through the κ-mechanism, for the destabilisation of the low-order, low-degree p-modes observed in EC 14026 pulsators (Charpinet et al. 1997). This additional ingredient in the constitutive physics of the models is therefore essential to reproduce the excitation of the pulsation modes. In addition, microscopic diffusion modifies sufficiently the stellar structure to induce significant changes to the pulsation periods themselves, thus impacting on the asteroseismic analysis (see Sect. 4.4). Four fundamental parameters are required to specify the internal structure of hot B subdwarf stars with the second-generation models: the effective temperature $T_{\rm eff}$, the surface gravity $\log g$ (traditionally given in terms of its logarithm), the total mass of the star M_*, and the logarithmic fractional mass of the hydrogen-rich envelope $\log q(\mathrm{H}) \equiv \log [M(\mathrm{H})/M_*]$. The latter parameter is intimately related to the more familiar parameter $M_{\rm env}$, which corresponds to the total mass of the H-rich envelope[1].

In a second step, we use two efficient codes based on finite element techniques to compute the pulsation properties of the model. The first one is an updated version of the adiabatic code described in detail in Brassard et al. (1992). It is used as an intermediate (and necessary) step for obtaining estimates for the pulsation mode properties (periods and eigenfunctions) that are then used as first guesses in the solution of the full, nonadiabatic set of nonradial oscillation equations. The second one is an improved version of the nonadiabatic code that has been described briefly in Fontaine et al. (1994) and which solves the nonadiabatic eigenvalue problem. It provides the necessary quantities to compare with the observations. To illustrate the type of quantities that are derived from the whole process, we provide, in Table 3, a typical output of the nonadiabatic pulsation code that gives the pulsation properties of a given model. While it refers specifically to the optimal model (see the discussion in the next subsection), we only wish to emphasise the illustrative aspect of the theoretical results at this point. For each mode found in the chosen period interval, Table 3 gives the degree ℓ, the radial order k, the period $P_{\rm th}$ ($= 2\pi/\sigma_R$, where σ_R is the real part of the complex eigenfrequency), the stability coefficient σ_I (the imaginary part of the eigenfrequency), the logarithm of the so-called kinetic energy of the mode E, and the dimensionless first-order solid rotation coefficient $C_{k\ell}$. As is standard, our equilibrium stellar models are perfectly spherical, and each mode is $2\ell+1$ fold-degenerate in eigenfrequency.

For asteroseismic studies, the most important quantities derived from theoretical calculations are of course the periods of the modes. These are sensitive to the global structural parameters of a model which we seek to infer for a real star through a comparison with a set of observed periods. Because nonadiabatic effects on the periods are small (but included in our calculations), asteroseismology could very well be carried out at the level of the adiabatic approximation only. However, the stability coefficient, a purely nonadiabatic quantity, also provides useful information on the mode driving mechanism. A positive value of σ_I indicates that a mode is damped (or "stable"), and therefore that it should not be observable. A negative value of σ_I indicates that the mode is excited (or "unstable") in the model, and consequently that it may reach observable amplitudes. As illustrated in Table 3, modes are excited within a band of periods mostly associated with low-order acoustic modes (note, however, the presence of two excited low-order gravity modes). This is typical of our models of rapid sdB pulsators, especially for low surface gravities where low-order $k \sim 1$ gravity modes or mixed modes tend to become marginally driven. In terms of asteroseismology, it is of course within that bandpass that one would expect to find the observed periods of a real EC 14026 star and this important stability information justifies the use of full nonadiabatic calculations in our case. For its part, the kinetic energy is a secondary quantity in the present context. It provides a measure of the required energy to excite a mode of a given amplitude at the surface of a star. Finally, the rotation coefficient is useful for interpreting the fine structure in

[1] We stress that the parameter $M_{\rm env}$ commonly used in Extreme Horizontal Branch stellar evolution includes the mass of the hydrogen contained in the thin He/H transition zone, while the parameter $M(\mathrm{H})$ in our models does not. They are related through $\log [M_{\rm env}/M_*] = \log [M(\mathrm{H})/M_*] + C$, where C is a small positive term, slightly dependent of the model parameters, determined by the mass of hydrogen that is present inside the He/H transition zone itself, and which can be computed after the fact in a converged model.

Table 3. Pulsation properties of the best-fit model solution and mode identification.

ℓ	k	$P_{\rm obs}$ (s)	$P_{\rm th}$ (s)	σ_I (rad/s)	Stability	$\log E$ (erg)	$C_{k\ell}$	$\Delta P/P$ (%)	ΔP (s)	Comments
0	5	...	157.185	$+4.926 \times 10^{-5}$	stable	39.922	...	...	...	
0	4	...	173.311	$+9.511 \times 10^{-6}$	stable	39.948	...	...	...	
0	3	...	201.344	-3.640×10^{-5}	unstable	40.227	...	...	...	
0	2	...	238.081	-3.397×10^{-5}	unstable	40.494	...	...	...	
0	1	...	294.372	-7.854×10^{-6}	unstable	41.098	...	...	...	
0	0	352.450	352.418	-8.974×10^{-7}	unstable	41.886	...	+0.009	+0.032	f_3: singlet
1	5	...	171.935	$+1.510 \times 10^{-5}$	stable	39.899	0.0068	...	...	
1	4	...	200.363	-3.608×10^{-5}	unstable	40.216	0.0064	...	...	
1	3	...	237.079	-3.455×10^{-5}	unstable	40.483	0.0089	...	...	
1	2	...	292.489	-8.095×10^{-6}	unstable	41.086	0.0140	...	...	
1	1	347.530	347.530	-5.044×10^{-7}	unstable	42.027	0.0306	0.000	0.000	f_2: triplet
1	1	...	597.094	-3.984×10^{-13}	unstable	47.011	0.4055	...	...	
2	5	...	169.233	$+2.636 \times 10^{-5}$	stable	39.848	0.0202	...	...	
2	4	...	194.678	-2.335×10^{-5}	unstable	40.275	0.1221	...	...	
2	3	...	206.733	-1.444×10^{-5}	unstable	40.645	0.2239	...	...	
2	2	...	236.054	-3.379×10^{-5}	unstable	40.486	0.0114	...	...	
2	1	...	289.169	-8.455×10^{-6}	unstable	41.068	0.0071	...	...	
2	0	345.997	345.960	-1.200×10^{-7}	unstable	41.763	0.0130	+0.011	+0.037	f_1: doublet
2	1	378.461	378.465	-3.938×10^{-9}	unstable	44.025	0.0820	−0.001	−0.004	f_4: triplet

the Fourier domain in terms of slow rotation that lifts the $2\ell+1$ fold-degeneracy of the mode periods (see Sect. 4.6).

4.2. The search for the optimal model of Feige 48

With only four independent modes revealed by the Fourier analysis of our CFHT data, Feige 48 provides us with less seismic constraints on its internal structure than any other rapidly pulsating sdB star analysed so far. In particular, this is problematic in view of the fact that one must specify four main parameters to fully determine the stellar structure of an sdB star with our second-generation models. Adjusting four model parameters to match four observed periods will obviously lead to strong degeneracies of the eventual solutions. Exploratory searches in the four-dimensional model parameter space using our multimodal genetic algorithm (GA) optimisation code indeed confirmed that using solely the quality of the period match as a criterion to isolate a best-fit model is impossible in the present case due to the nature of the degeneracies (these will be illustrated below). Fortunately, one can rely on the additional constraints brought by spectroscopy to alleviate this difficulty. Consequently, in our seismic analysis of Feige 48, we followed a slightly different strategy than in our previous asteroseismic studies of EC 14026 stars (as in, e.g., Charpinet et al. 2005). We adopted the effective temperature of Feige 48 derived from our spectroscopic measurements, $T_{\rm eff}$ = 29 580 K, as our definitive, best estimate for this parameter. This choice is, indeed, well justified by the fact that the effective temperature is much more accurately derived through spectroscopic means than through asteroseismic investigations for sdB stars. Thus, we performed a global search in the reduced, three-dimensional parameter space defined by the three remaining parameters $\log g$, M_*, and $\log q$(H) with our multimodal genetic algorithm optimisation code. The GA code was used to localise potential regions where solutions may exist. Initial boundaries of the search domain were defined as follows: $5.30 \leq \log g \leq 5.55$ for the surface gravity parameter (as $T_{\rm eff}$ was kept constant at the spectroscopic value), and $-5.0 \leq \log q({\rm H}) \leq -2.0$, $0.43 \leq M_*/M_\odot \leq 0.53$ for the structural parameters.

These limits were set according to the current spectroscopic estimate for the surface gravity of Feige 48. Constraints on the two other parameters M_* and $\log q$(H) rely on stellar evolution theory. The evolutionary calculations of Dorman et al. (1993) indicate that hot B subdwarfs are core helium burning stars on the Extreme Horizontal Branch that evolve as "AGB-Manqué" objects. According to these calculations, their possible masses are found in a narrow range $0.40{-}0.43 \lesssim M_*/M_\odot \lesssim 0.53$, with a somewhat uncertain lower limit related to the minimum mass required to ignite helium and a more sharply defined upper limit above which the models evolve to the AGB. More recently, however, Han et al. (2003) suggested, in their investigation of various binary evolution scenarios for the formation of sdB stars, a somewhat larger distribution of masses among these stars. Although these authors derived mass distributions which are strongly peaked around the canonical value of $\sim$0.47 $M_\odot$, they suggest that the mass of an sdB star could be as low as $\sim$0.30 $M_\odot$ if formed through the Roche lobe overflow channel or as high as $\sim$0.70 $M_\odot$ if formed through the merger channel. In the present study, in order to reduce computation time, we first adopted the "canonical" mass range. At the outset, it turns out that the viable asteroseismic solution lies within this domain. Nonetheless, in order to explore with asteroseismology the possibility of a lower or higher mass for Feige 48, some calculations were extended accordingly in the

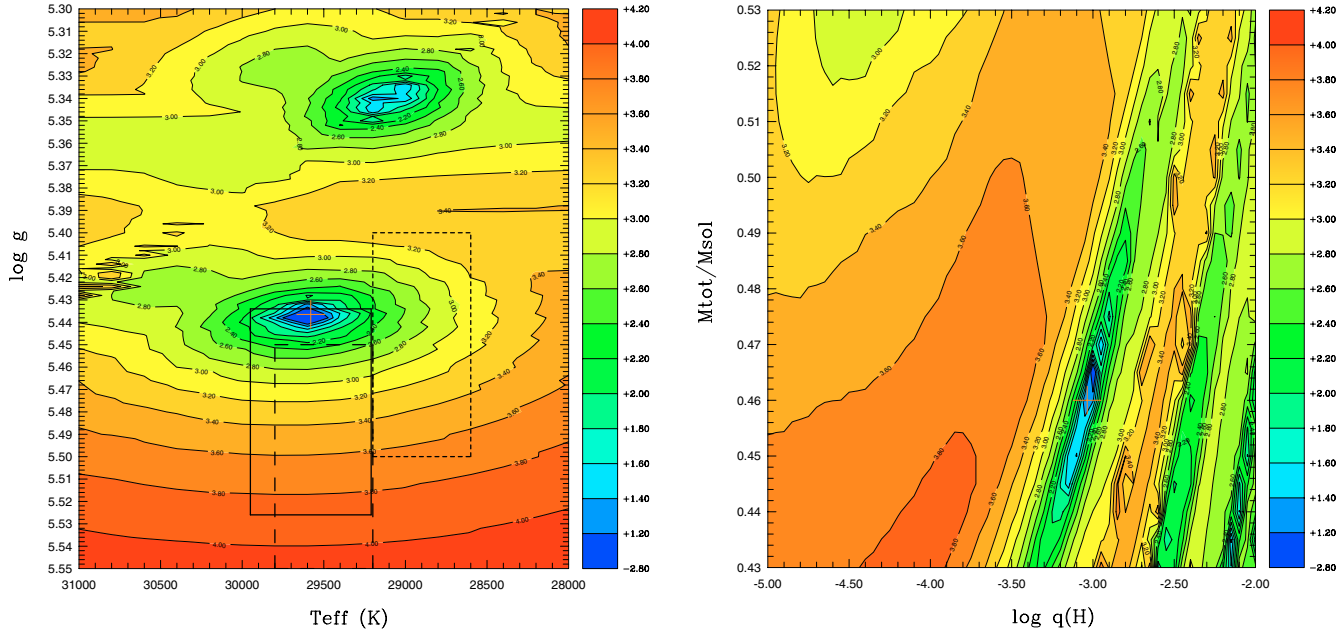

Fig. 8. *Left panel*: slice of the $\overline{\chi}^2$-function (in logarithmic units) along the $\log g - T_{\rm eff}$ plane at fixed parameters M_* and $\log q$(H) set to their optimal values found for the best-fit model solution ($M_* = 0.4600\ M_\odot$ and $\log q$(H) $= -3.0353$). The solid-line rectangle materialises our spectroscopic estimate with its uncertainties for the atmospheric parameters of Feige 48, while the dotted-line and the dashed-line rectangles represent the Koen et al. (1998) and Heber et al. (2000) spectroscopic measurements, respectively. The red cross indicates the position of the best fit solution. *Right panel*: slice of the $\overline{\chi}^2$-function (in logarithmic units) along the $M_* - \log q$(H) plane at fixed parameters $T_{\rm eff}$ and $\log g$ set to their optimal values found for the first best fit model solution ($T_{\rm eff} = 29\,580$ K and $\log g = 5.4365$). The red cross indicates the position of the best fit solution considered.

course of our detailed analysis (see below). Finally, the range of possible values for the last parameter $\log q$(H), which is related to the mass of the H-rich envelope, was chosen according to the work of Dorman et al. (1993) in order to fully map the region of the $\log g - T_{\rm eff}$ plane where sdB stars are found.

For the pulsation calculation step, we considered all the modes (be it of p-, f-, or g-type) of degree $\ell = 0$ up to $\ell = 2$ with periods in the range 100–800 s, i.e., covering amply the range of periods observed in Feige 48. The choice for the upper limit of the ℓ value was motivated according to the discussion of Charpinet et al. (2005), i.e., it corresponds to the minimum value of the degree ℓ that permits to account for the mode density in the observed period range. The usual argument to limit the value of ℓ above which modes are no longer observable is geometric cancellation on the visible disk of the star, which naturally favours a priori values of $\ell = 0$, 1, and 2 in pulsating stars in general. We note, however, that the mode densities and period distributions seen in several well-observed EC 14026 stars such as KPD 1930+2752, PG 1605+072, PG 1047+003, PG 0014+067, and PG 1219+534 force us to consider modes with higher ℓ values ($\ell = 3$, or even $\ell = 4$ in some cases). Otherwise, there would not be enough theoretical modes available in the observed period window to account for the observations. For Feige 48, modes up to $\ell = 2$ are sufficient to account for the observed mode density. We cannot rule out completely the presence of the $\ell = 3$ modes (or perhaps even a mode of higher degree) with an unusually high intrinsic amplitude in the light curve of this star. Our approach explicitly excludes this possibility, however, and we seek to interpret the period distribution in that star solely in terms of $\ell = 0$–2 modes.

Within the three-dimensional search domain specified, the GA code identified two families of solutions that offer good matches for the four observed periods, although one family distinguishes itself at the quantitative level. Indeed, the optimal model corresponding to the first family of solutions is found at $T_{\rm eff} = 29\,580$ K (the value derived from spectroscopy), $\log g = 5.4365$, $\log q$(H) $= -3.0353$, and $M_* = 0.4600\ M_\odot$, and boasts an almost perfect merit function of $\overline{\chi}^2 \simeq 2.4 \times 10^{-3}$. In comparison, the optimal model associated with the second family of solutions is localised at $T_{\rm eff} = 29\,580$ K (again, the value from spectroscopy), $\log g = 5.3339$, $\log q$(H) $= -3.2024$, and $M_* = 0.4545\ M_\odot$, with a value of $\overline{\chi}^2 \simeq 1.066$. While the latter corresponds to a quite acceptable fit on an absolute scale, that value is some 444 times larger than what is found for the first case and, therefore, argues very strongly against the possibility that the second family of solutions corresponds better to reality. To reinforce this conclusion, we show below that the available spectroscopic determinations of the surface gravity effectively rule out the second set of solutions. Note that in the evaluation of $\overline{\chi}^2$ (see Eq. (1) of Charpinet et al. 2005), we have chosen a constant global weight factor set to the value $\sigma_i = 1$ (a choice that has no impact on the location of the best-fit solutions).

Maps displayed in Fig. 8 illustrate the shape of the $\overline{\chi}^2$-function (shown as isocontours of constant value of $\log\overline{\chi}^2$) in the vicinity of the first potential solution (our preferred solution), whose exact location according to the GA code is indicated by a red cross. This figure respectively shows slices of this function along the $\log g - T_{\rm eff}$ plane (at fixed parameters M_* and $\log q$(H) set to their optimal values) and along the $M_* - \log q$(H) plane (at fixed parameters $T_{\rm eff}$ and $\log g$

set to their optimal values). Best fitting models corresponding to low values of $\overline{\chi}^2$ appear as dark blue regions, while red areas indicate regions of the model parameter space with high values of $\overline{\chi}^2$, i.e., where theoretical periods computed from models do not fit well the observed periods. Considering the logarithmic scale used to represent the merit function on these plots, we point out that the blue regions are very well-defined minima. In the left panel of Fig. 8, two regions of minimum $\overline{\chi}^2$-value corresponding to the two families of solutions mentioned above are apparent. Note that the region at low surface gravity is shifted to a cooler effective temperature because, for this map, the fixed parameters $\log q(\mathrm{H})$ and M_* are set to the optimal values corresponding to the solution found at higher surface gravity. This shift is due to the other type of degeneracy – which we will illustrate below – that originally forced us to restrict our search in the parameter space using the spectroscopic value of $T_{\rm eff}$. Despite the existence of two potential families of asteroseismic solutions, all the current spectroscopic measurements and their associated errors (shown as rectangles in Fig. 8) available for Feige 48 clearly indicate that the solution at higher surface gravity (i.e., the first family of solutions) should be the preferred one. Since this is also the one showing the smallest values of $\overline{\chi}^2$, we therefore readily adopted this family of models located near $\log g \sim 5.44$ as the best candidate solution that would reproduce simultaneously the four independent periods observed in Feige 48, while being consistent with the spectroscopy. Figure 8 also shows that, at higher surface gravities, the $\overline{\chi}^2$ values rise dramatically, indicating that models in this area are increasingly bad at providing a match of the observed periods. This behaviour is simply explained by the fact that for models with $\log g$ higher than ∼5.44, several or all observed periods would have to be fitted to low-order gravity modes. However, the g-modes have a much lower period density than the p-modes in this period range, which is incompatible with the observed mode density. Hence, we find it impossible to provide a simultaneous match to the observed periods of Feige 48 with seismic models of surface gravity higher than $\log g \sim 5.44$.

Beyond the best-fit model degeneracy discussed above, a more subtle type of degeneracy of the asteroseismic solution among the chosen family of models exists. This degeneracy occurs when a change in one of the model parameters is almost exactly compensated by a change in another model parameter such that the computed periods remain unmodified. This phenomenon occurs in our analysis of Feige 48 at two levels. First, there is a correlation between the $\log q(\mathrm{H})$ and $T_{\rm eff}$ parameters. From the best-fit model uncovered, changing the value of $\log q(\mathrm{H})$ while keeping M_* constant and set to its optimal value generates, in the $\log g - T_{\rm eff}$ plane, a shift in position of the local minimum which mainly follows the effective temperature axis (a tiny shift also occurs in $\log g$). This trend is illustrated with the map provided in Fig. 9, which shows the "projection" of the $\log q(\mathrm{H})$ axis onto the surface gravity-effective temperature plane. More precisely, the value associated to each grid point shown on this map is the minimum value found among all the values of the $\overline{\chi}^2$-function computed at fixed $T_{\rm eff}$, $\log g$ (set to the values associated with the considered grid point), and M_* (set to its optimal value, that is $M_* = 0.4600\ M_\odot$) but with the parameter $\log q(\mathrm{H})$ varying within the limits of the specified search domain, i.e., between $\log q(\mathrm{H}) = -5.0$ and -2.0. The various families of solutions identified previously now appear simultaneously as (blue) parallel valleys of low $\overline{\chi}^2$ in the $\log g - T_{\rm eff}$ plane. The labelled axis positioned along the valley associated with the preferred solution indicates the position of the local minimum of $\overline{\chi}^2$ as a function of $\log q(\mathrm{H})$. There is a clear, monotonic trend showing that this minimum shifts from higher effective temperatures (e.g., $T_{\rm eff} \sim 30\,700$ K for $\log q(\mathrm{H}) \sim -3.2750$) to lower $T_{\rm eff}$ (∼28 200 K for $\log q(\mathrm{H}) \sim -2.7500$) as the envelope mass of the star increases (i.e., $\log q(\mathrm{H})$ increases). There is no degradation in the quality of the period fit over the entire range considered for the $\log q(\mathrm{H})$ parameter. Clearly in the case of Feige 48, the impact of changing the value of $\log q(\mathrm{H})$ on the theoretical modes fitted to the observed periods can be completely compensated by an adequate change of $T_{\rm eff}$ (and $\log g$ to a much lesser extent). This leads to a line degeneracy in the $\overline{\chi}^2$-function along which models provide comparable best-fit solutions of the periods.

A similar map was constructed to visualise the "projection" of the M_*-axis onto the $\log g - T_{\rm eff}$ plane. It is shown in Fig. 10. The parameter $\log q(\mathrm{H})$ was kept constant (set to its optimal value of $\log q(\mathrm{H}) = -3.0353$) and the total mass was varied between $M_* = 0.70\ M_\odot$ and $M_* = 0.30\ M_\odot$ (note that we have extended the search domain to higher and lower masses). Again, the map indicates clearly that a correlation exists between the parameter M_* and the parameters $T_{\rm eff}$ and, to a lesser extent, $\log g$. A change in M_* generates a shift in both $T_{\rm eff}$ and $\log g$ of the position of the $\overline{\chi}^2$ minimum. And again, we observe no degradation of the quality of the period fit over the entire range considered for the M_* parameter. Therefore, the impact of changing the value of M_* on the theoretical modes fitted to the observed periods can be completely compensated by an adequate change of both $T_{\rm eff}$ and $\log g$, leading to another line-degeneracy in the $\overline{\chi}^2$-function. This is well illustrated in Fig. 10 by the presence of two long and flat valleys of minimum value of $\overline{\chi}^2$ associated with both families of solutions. The labelled axis plotted along the valley of minimum $\overline{\chi}^2$ indicates the position of the best-fit solution in the $\log g - T_{\rm eff}$ plane for the given value of the total mass. The correlation between M_* and ($T_{\rm eff}$, $\log g$) is monotonic as the effective temperature and surface gravity of the solution decreases when the total mass decreases. For instance, a value of $M_* = 0.4875\ M_\odot$ places the minimum of $\overline{\chi}^2$ near $T_{\rm eff} \sim 30\,850$ K and $\log g \sim 5.446$, while a value of $M_* = 0.4300\ M_\odot$ places it near $T_{\rm eff} \sim 28\,200$ K and $\log g \sim 5.428$. Note that the correlation with the effective temperature is much stronger than the correlation with the surface gravity parameter. Of course, this trend extends beyond the limits provided in Fig. 10, and models with lower (higher) masses lead to even cooler (hotter) solutions. Interestingly, the same trend was noted in the analysis of the rapid sdB pulsator PG 1219+534 (Charpinet et al. 2005).

Since, one cannot discriminate between the models belonging to the first family on the basis of their $\overline{\chi}^2$-values alone, this justifies a posteriori our use of spectroscopy to lift these degeneracies by fixing the effective temperature derived from the analysis of our medium-resolution, high signal-to-noise ratio

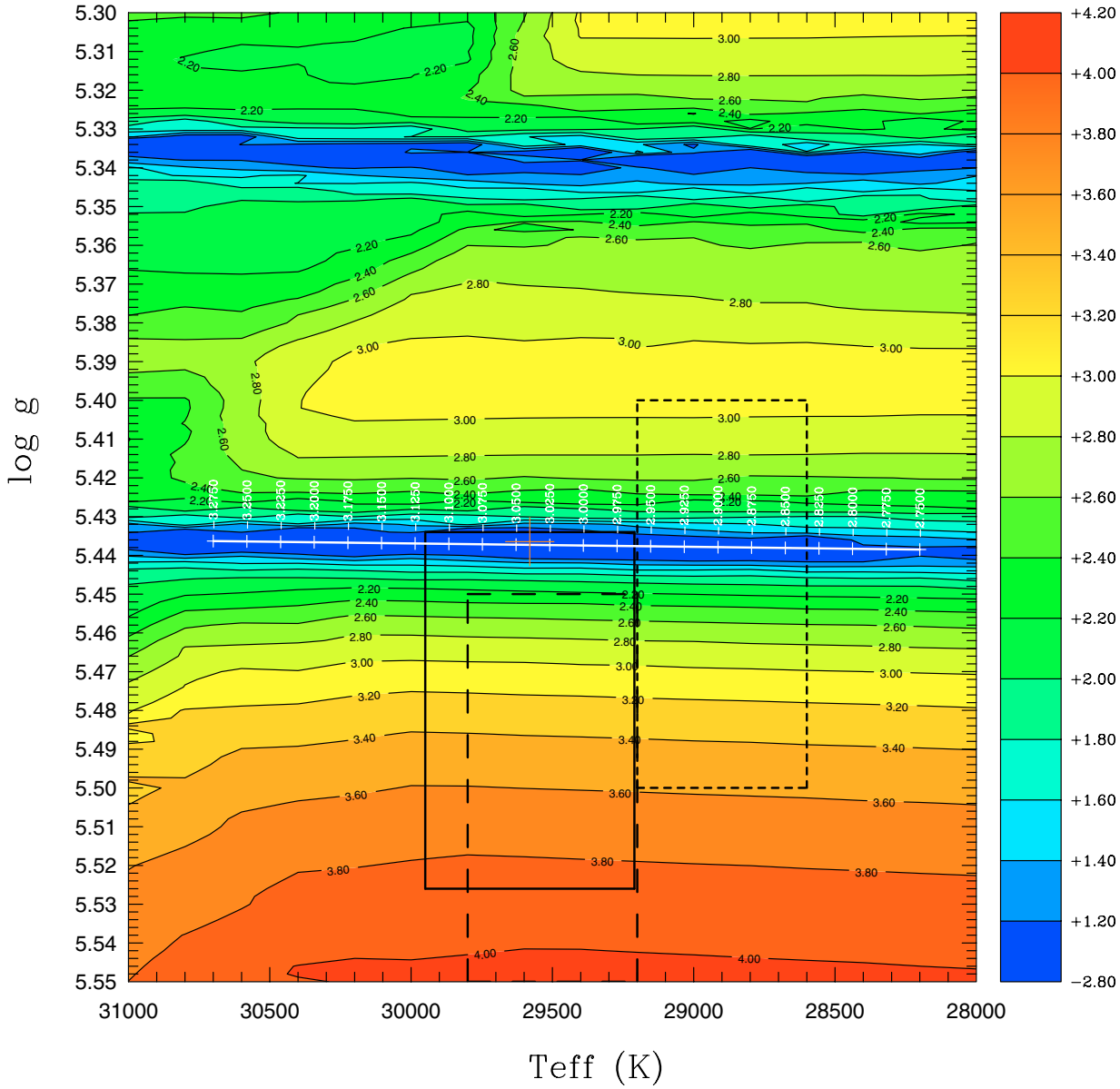

Fig. 9. Slice of the "projected" $\overline{\chi}^2$-function (in logarithmic units) along the $\log g - T_{\rm eff}$ plane at fixed parameter M_* set to its optimal value found for the best-fit model solution ($M_* = 0.4600\ M_\odot$). The projected, $\log q$(H) parameter was varied between −2.0 and −5.0 (by steps of 0.025). The labelled axis positioned along the valley of minimum $\overline{\chi}^2$ indicates the exact location of the local minimum of $\overline{\chi}^2$ for the mentioned value of $\log q$(H) (see text for further details). The solid-line rectangle materialises our spectroscopic estimate with its uncertainties for the atmospheric parameters of Feige 48, while the dotted-line and the dashed-line rectangles represent the Koen et al. (1998) and Heber et al. (2000) spectroscopic measurements, respectively.

MMT spectrum (the solid-line rectangles in Figs. 9 and 10). It allows us to select the appropriate section along the lines of degeneracy which presumably corresponds to the "correct" solution. Of course, the necessity to rely on the spectroscopic measurement of $T_{\rm eff}$ to uniquely derive the total mass and the mass of the H-rich envelope of Feige 48 from asteroseismology means, unfortunately, that these parameters cannot be measured independently of $T_{\rm eff}$ for that star.

Of interest in the context of binary evolution scenarios proposed to form hot B subdwarf stars, we find that the low-mass (high-mass) models consistent with the observed periods of Feige 48 would require effective temperatures which are significantly cooler (hotter) than currently measured by spectroscopic means. Therefore, those solutions can clearly be rejected on the basis of consistency between spectroscopy and asteroseismology. Remarkably, the mass derived for Feige 48, which is compatible with the spectroscopically measured effective temperature, is found to be consistent with the canonical value for Extreme Horizontal Branch objects. We also note at this point that best-fit model candidates for the observed periods of Feige 48 do all correspond to models with relatively thick H-rich envelopes. In our search, no acceptable asteroseismological fit has been found for models with thin envelopes, i.e., with low values of the parameter $\log q$(H). This is in contrast with the values indicative of thin envelopes derived for the hotter sdB pulsators PG 0014+067 (Brassard et al. 2001)

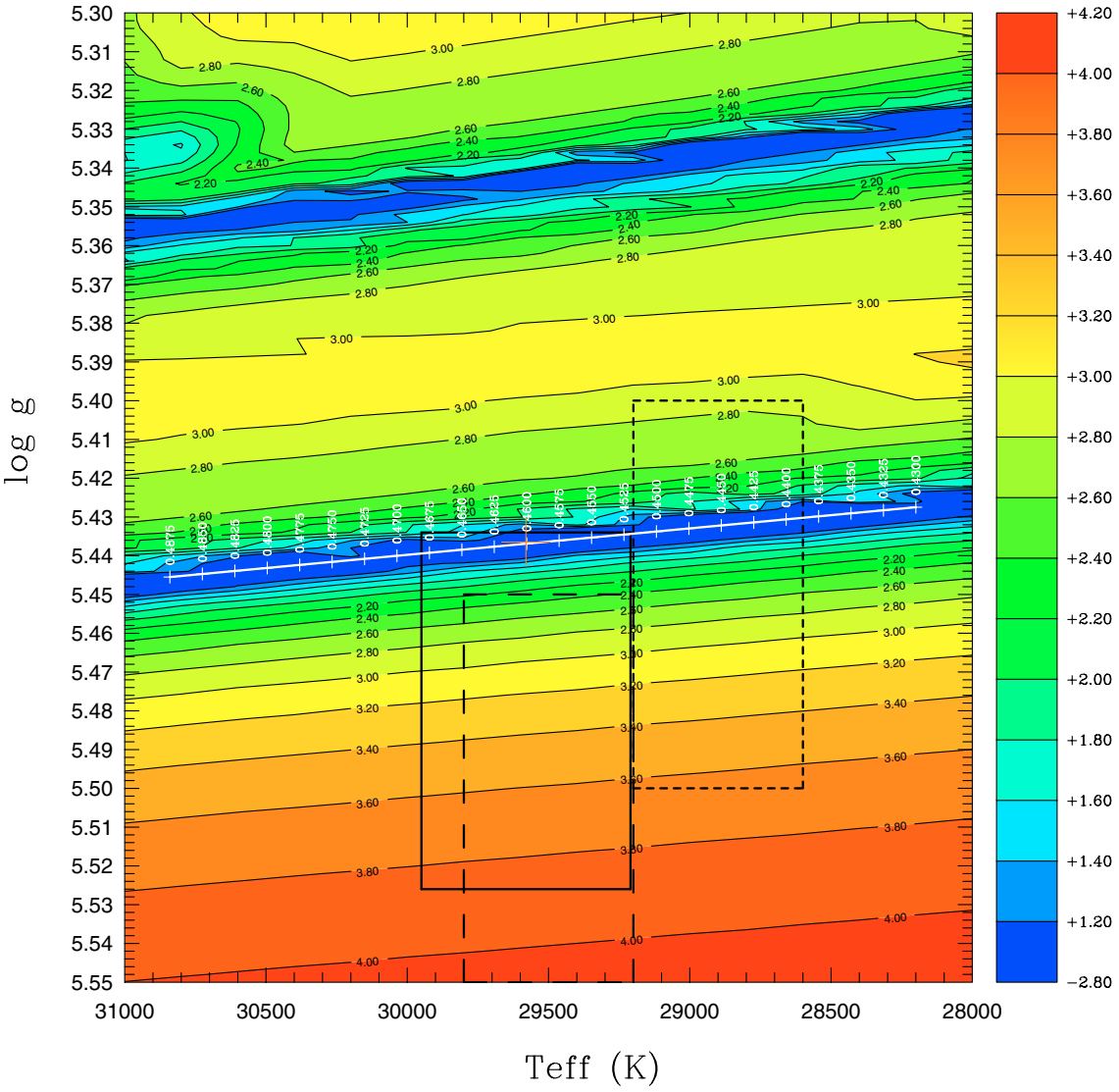

Fig. 10. Slice of the "projected" $\overline{\chi}^2$-function (in logarithmic units) along the $\log g - T_{\rm eff}$ plane at fixed parameter $\log q$(H) set to its optimal value found for the best-fit model solution ($\log q$(H) = −3.0353). The projected, M_* parameter was varied between 0.30 $M_\odot$ and 0.70 $M_\odot$ (by steps of 0.0025 $M_\odot$). The labelled axis positioned along the valley of minimum $\overline{\chi}^2$ indicates the exact location of the local minimum of $\overline{\chi}^2$ for the mentioned value of M_* (see text for further details). The solid-line rectangle materialises our spectroscopic estimate with its uncertainties for the atmospheric parameters of Feige 48, while the dotted-line and the dashed-line rectangles represent the Koen et al. (1998) and Heber et al. (2000) spectroscopic measurements, respectively.

and PG 1219+534 (Charpinet et al. 2005). Hence, this result agrees quite well, at least qualitatively, with the expected trend derived from standard stellar evolution theory which states that EHB stars should have lower effective temperatures with increasing H-rich envelope masses.

4.3. Period fit and mode identification

The optimal model isolated in the previous subsection provides the best simultaneous period match of the four independent periods detected in Feige 48 and leads to the identification of the pulsation modes involved in the luminosity variations observed in that star. We recall that our global optimisation method does not rely on any previous assumption concerning the values of the degree ℓ and the radial order k of the modes being observed except for the "$2\ell+1$ splitting rule" discussed above[2]. The mode identification appears instead naturally as a solution (or prediction) of the double-optimisation procedure. Details on the derived period fit and mode identification for Feige 48 are given in Table 3 (a graphical representation of it is also shown in Fig. 11). In addition to the quantities that reflect the properties of the nonradial modes computed from the best-fit model (already described in Sect. 4.2), Table 3 provides the derived distribution of the observed periods ($P_{\rm obs}$) as these were matched to the theoretical periods ($P_{\rm th}$). Again, this distribution is the one that minimises χ^2, the sum of the squared difference

[2] Note, in this context, that additional calculations ignoring this constraint have recovered the exact same optimal model, so it would appear that the constraint based on mode splitting is not of high value in our particular case here.

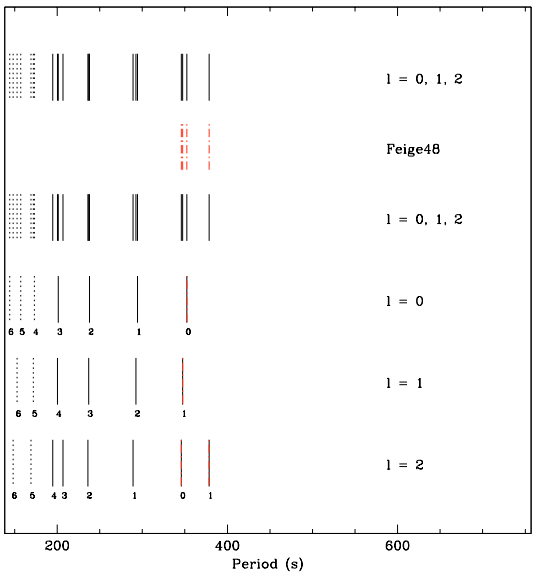

Fig. 11. Comparison of the observed period spectrum of Feige 48 (*thick dashed-dotted-line red segments*) with the theoretical pulsation spectrum of the optimal model. For the latter spectrum, *solid-line segments* indicate excited modes, while *dotted-line segments* correspond to damped modes. All pulsation modes with $\ell = 0$, 1, and 2 in the period interval 140−400 s are illustrated. The values of the radial order index k are also indicated for each mode. At this scale, the match is perfect.

between the observed periods and their assigned theoretical periods for that model (see Charpinet et al. 2005). The relative and absolute differences in period, $\Delta P/P$ (in %) and ΔP (s), for each pair ($P_{\rm obs}$, $P_{\rm th}$) are also given in this table.

We find that the simultaneous fit of the four independent periods of Feige 48 obtained with the selected optimal model is outstanding by current standards. The average relative dispersion between the fitted periods is only $\overline{\Delta P/P} \sim 0.005\%$ and the worst difference is ∼0.011%. On an absolute scale, the average dispersion between the periods is $\overline{\Delta P} \sim 0.018$ s, less than the mean accuracy on the observed periods of ∼0.027 s. This means that, for the first time, we have reproduced the observed periods of an EC 14026 pulsator at their level of accuracy. This accurate and simultaneous fit is superior in quality to the results achieved by Brassard et al. (2001; $\overline{\Delta P} \sim 1$ s) for the star PG 0014+067 and by Charpinet et al. (2005; $\overline{\Delta P} \sim 0.8$ s) for the star PG 1219+534, although we must point out that more modes (13 and 9, respectively) had to be fitted simultaneously in these analyses (compared to only 4 in the present case). The fact that the accuracy at which the observed periods are reproduced appears to be a function of the number of modes available indicates to us that our equilibrium models describing the structure of sdB stars still suffer from imperfections that leave significant room for improvement, on an absolute scale, in reproducing all the current observations. This is, of course, one of the goals to pursue in future asteroseismic studies of sdB pulsators.

We find furthermore that the four observed independent periods all fall within the predicted band of instability, as it is clearly apparent in Table 3. Hence, the model solution derived from the global optimisation procedure is also fully consistent with the predictions of nonadiabatic pulsation theory applied to our second generation models of pulsating hot B subdwarfs. Remarkably, the period f_3 identified as a singlet is identified as a radial ($\ell = 0$) mode, as one might have expected from the apparent lack of fine structure associated with this mode. Similarly, the doublet f_1 and the two triplets f_2 and f_4 are found to be nonradial $\ell = 1$ and 2 modes. The modes are identified as low-order ($k = 0$, 1) f- and p-modes, with the interesting exception of f_4 associated with an excited low-order ($k = 1$), $\ell = 2$ g-mode. Having low-order gravity waves and/or mixed modes excited in EC 14026 stars of lower surface gravity, such as Feige 48, is not uncommon according to current models.

As illustrated in Table 3 and Fig. 11, modes of degree up to $\ell = 2$ only are needed to account for the mode density observed in Feige 48, while several other sdB pulsators require modes of degree up to $\ell = 3$ (or even $\ell = 4$). Interestingly, as a test of the robustness of this result, we performed a global search with the GA code allowing this time for modes of degree up to $\ell = 3$ to be matched to the observed periods. Remarkably, the preferred solution converged toward the same model and mode identification presented in Table 3 and Fig. 11, i.e., none of the observed periods was assigned to a $\ell = 3$ mode. This is strong indication that no mode of degree larger than $\ell = 2$ is currently seen in the pulsation spectrum of Feige 48.

In addition, we note that all the observed modes tend to cluster near the low radial order (low-k, or long-period) boundary of the predicted band of instability. Similar mode distributions are actually seen in PG 0014+067 and in PG 1219+534 (see Brassard et al. 2001 and the discussion of Charpinet et al. 2005). Similarly to other EC 14026 stars analysed so far, we find no firmly established hierarchy of the mode amplitude as a function of ℓ for the modes identified in Table 3. One would naively expect, at least statistically, some trend of amplitude attenuation when ℓ increases, due to geometric cancellation effects. We find instead that the f_3 mode assigned to $\ell = 0$ has an amplitude of 0.116%, the central component of the f_2 triplet assigned to $\ell = 1$ has the largest amplitude at 0.640%, and that the f_1 and f_4 modes, both assigned to $\ell = 2$, have amplitudes of 0.111% and 0.131%, respectively (see Table 2). Hence, it would appear that simplistic argumentation based on expected mode visibility to rule out a priori the possible detection of modes with ℓ values of 3 or 4 in pulsating sdB stars should be avoided. In addition, Feige 48 is expected to be seen nearly pole-on (see Sect. 4.6). For a star seen nearly pole-on, geometric cancellation effects are much stronger on the $m \neq 0$ components of a multiplet and, consequently, the $m = 0$ component is expected to dominate in amplitude. This trend is observed, at least qualitatively, with the multiplets detected in the light curve of Feige 48. However, because intrinsic amplitudes of the various components are not known a priori and may be significantly different from one mode to the other (as seems to be the case in EC 14026 stars in general), a quantitative check of these trends is not possible at this stage. All these issues related to mode amplitudes are beyond the realm of linear theory and only a nonlinear approach to the pulsation phenomenon will be able to address properly these questions.

To end up this subsection, we stress that the (k, ℓ) values attributed to the periods observed in Feige 48 constitute a prediction of our seismic analysis that can ultimately be independently tested observationally. A promising avenue for independent mode identification resides in multicolour photometry (as opposed to one colour, "white light" photometry used, for instance, in this study). It is well known from stellar pulsation theory that the apparent amplitude of a nonradial oscillation mode is a function of wavelength. Moreover, how this amplitude changes with wavelength depends on the degree ℓ of the mode. Consequently, measuring relative amplitude ratios of modes observed at different wavelengths allows, in principle, the identification of their degree ℓ. Such independent evaluations of the geometry of the modes would obviously provide important tests of our seismic analyses. Some very encouraging results based on that technique have been presented recently by Jeffery et al. (2004), including the suggested identification of a mode with $\ell = 4$ in the hot pulsating sdB star KPD 2109+4401.

4.4. Comparison with Reed et al. (2004)

Reed et al. (2004) have attempted to match the periods of Feige 48 using standard evolutionary models of extreme horizontal branch stars. Those are comparable, for instance, to the "first generation" models used by Charpinet et al. (2000, 2002b). Due to the lower sensitivity of the observations upon which they based their analysis, only three independent periods (compared to the four identified in the present study) were available to them for constraining the models. These periods are indicated in Table 4 along with their identified ℓ and k values according to the best-match model proposed by these authors. The structural parameters of their model are $M_* = 0.4725\ M_\odot$, $M_{\rm env} = 0.0025\ M_\odot$, $T_{\rm eff} = 29\,635$ K, and $\log g = 5.518$. Their model differs from our second generation models (besides the fact that it is an evolved and not a static structure) in that it does not incorporate the nonuniform profile of iron in the envelope expected from microscopic diffusion processes. This model was computed with the assumption of uniform solar metallicity in the envelope of the star, as is standard in current EHB evolution calculations. For comparison purposes, we produced a static structure assuming uniform solar ($Z = 0.02$) metallicity and using the same parameters as the model of Reed et al. (2004). As expected, the periods derived for both models are very close (see Table 4), the small differences in period being accountable for the slight differences that exist in the microphysics used to build the two models. The fact that, with very little effort, we can reproduce rather well the computed periods of Reed et al. (2004) confirms our claim that evolutionary structures are not essential for precise asteroseismology of EC 14026 stars and can be advantageously replaced by static structures. This is discussed in more detail in Charpinet et al. (2002a). Of higher interest, however, is the observation of Reed et al. (2004) that their best-fit model is not able to reproduce satisfactorily the three available periods simultaneously. Their fit to the 352.40 s and 347.56 s modes is quite good, but they could not find in their theoretical period spectrum a mode with $\ell = 0$, 1, or 2 with a period close to 378.50 s. Since the authors did not allow the latter mode to have $\ell = 3$ (a period of 374.0 s is present in their theoretical spectrum with $\ell = 3$), they suggested this "could indicate that (their) current models do not include enough physics to be accurate". We argue that, in fact, the 378.5 s mode can be modelled and reconciled with $\ell = 2$ if the missing ingredient is *radiative levitation.*

Table 4. Comparison with the model of Reed et al. (2004).

ℓ	k	Observed Period	Reed et al. (2004)	Static model $Z = 0.02$	Static model Z nonuniform
0	0	352.40 s	352.3 s	349.5 s	315.5 s
1	1	347.56 s	347.4 s	347.5 s	310.1 s
3	0	378.50 s	374.0 s	375.3 s	396.6 s

In order to illustrate the impact of microscopic diffusion on the pulsation modes, we computed the periods for another static model keeping unchanged the stellar parameters given above, but using, this time, the nonuniform profile of iron abundance predicted by the equilibrium theory between radiative levitation and gravitational settling. The result, also given in Table 4, clearly shows that the pulsation periods are, indeed, significantly modified by the chemical stratification induced by diffusion in the envelope of the star. This is directly linked to the significant modifications in the thermal structure of the star, through the opacity of the gas in the envelope, that are triggered by local accumulation or depletion of heavy metals (in particular, iron) to which the periods of pulsation modes are sensitive. Hence, the obvious consequence is that radiative levitation is definitely a *crucial* ingredient that *must* be taken into account in the modelling of pulsating sdB stars for the purpose of accurate asteroseismology. Quantitative asteroseismology of sdB stars is simply not possible with standard evolutionary models, and this must be realised. The fact that our seismic analysis using the second generation models (which include the nonuniform profiles predicted by diffusion) allowed us to find a solution that provides an exquisite, simultaneous match to the four independent periods that we have detected in Feige 48 from the CFHT light curves strengthens this conclusion.

4.5. Structural parameters of Feige 48

The model that has been isolated and which best represents the observed properties of Feige 48, from both the spectroscopy and asteroseismology standpoints, leads to the determination of the fundamental parameters that define the structure of this hot pulsating B subdwarf. A first set of primary quantities corresponding to the main model parameters is naturally derived from this exercise. These primary parameters are the effective temperature $T_{\rm eff}$, the logarithm of the surface gravity $\log g$, the total mass M_*, and the mass of the hydrogen-rich envelope through the quantity $\log q({\rm H}) + C = \log (M_{\rm env}/M_*)$. A set of secondary parameters then follows from the values obtained for the primary quantities. These secondary parameters are the radius R (as a function of M_* and g), the luminosity L (as a function of $T_{\rm eff}$ and R), the absolute magnitude M_V (as a function of g, $T_{\rm eff}$, and M_* in conjunction with the use of detailed model atmospheres), and the distance from Earth d (as a

Table 5. Inferred properties of Feige 48 ($V = 13.46 \pm 0.02$)

Quantity	Estimated value
$\log g$	5.4365 ± 0.0060 (0.11%)
$T_{\rm eff}$ (K)	29580 ± 370 (1.25%)
$M_*/M_\odot$	0.460 ± 0.008 (1.74%)
$\log (M_{\rm env}/M_*)$	−2.97 ± 0.09 (3.03%)
$R/R_\odot$ (M_*, g)	0.2147 ± 0.0034 (1.58%)
$L/L_\odot$ ($T_{\rm eff}$, R)	31.62 ± 2.58 (8.16%)
M_V (g, $T_{\rm eff}$, M_*)	3.961 ± 0.062 (1.57%)
$d(V, M_V)$ (pc)	794 ± 30 (3.8%)
$P_{\rm rot}$ (h)	9.44 ± 1.18 (12.5%)
$V_{\rm eq}(R, P_{\rm rot})$ (km s^{-1})	27.6 ± 3.9 (14.1%)
i (°)	≤10.4 ± 1.7

function of V and M_V). The determination of the rotation period $P_{\rm rot}$, equatorial rotation velocity $V_{\rm eq}$ (as a function of R and $P_{\rm rot}$), and inclination angle i could also be achieved due to the presence of fine structure in the frequency spectrum of Feige 48 which can be interpreted in terms of the slow rotation of the star (see Sect. 4.6). The values derived for all these quantities are summarised in Table 5.

An essential ingredient of our asteroseismic studies is an evaluation of the uncertainties associated with the parameters derived for the optimal model. However, the small number of available independent modes (four only) compared to the number of free parameters necessary to specify the models (four also), prevents us from using the method based on the modelling of the χ^2-hypersurface in the vicinity of the best-fit solution introduced in Brassard et al. (2001; see also Charpinet et al. 2005). We instead considered, as an alternative method to provide estimates of the uncertainties, the relatively strong constraint brought by spectroscopy on the determination of the effective temperature. Using projection maps of the merit function such as those illustrated in Figs. 9 and 10, one can delimit the domain of acceptable values for all model parameters according to the limits (i.e., the evaluated errors) imposed by spectroscopy on the $T_{\rm eff}$ values. A close examination of these maps indicates that, at the 68.3% confidence level, the error estimates associated with the four primary parameters of Feige 48 (i.e., $\log g$, $T_{\rm eff}$, M_*, and $\log [M_{\rm env}/M_*] = \log q[{\rm H}] + C$) correspond to the values given in Table 5. Uncertainties on the secondary quantities are then easily derived from the values obtained for the primary parameters. We find that these error estimates are of the same order as those derived for other well studied sdB pulsators from the method of Brassard et al. (2001).

As noted in previous analyses of EC 14026 stars, a significant contribution of asteroseismology to the study of sdB stars is the ability to derive values for the surface gravity $\log g$ with unprecedented accuracy, i.e., improved by a factor of ∼10 compared to current spectroscopic measurements, typically. This reflects the fact that the p-mode periods are particularly sensitive to the gas density which strongly affects the speed at which acoustic waves propagate in the stellar interior (i.e., the sound speed). How dense and compact a sdB star is, of course, largely depends on the $\log g$ parameter (see, e.g., Charpinet et al. 2002a). On the other hand, the effective temperature is not well constrained, due in part to the fact that the p-mode periods are relatively insensitive to this parameter in sdB stars, but also because solution degeneracies may prevent one from uniquely measuring that quantity through asteroseismology alone. In this context, spectroscopy provides a much more accurate method to measure $T_{\rm eff}$ and allows one to lift eventual degeneracies in the asteroseismic solutions. Hence, again, we stress that both methods have complementary roles to play in this respect. Asteroseismology also allows for the determinations at an interesting level of accuracy of fundamental structural quantities, such as the total mass and the thickness of the outer H-rich envelope in hot B subdwarfs, two key parameters for testing theories of formation and evolution of stars on the Extreme Horizontal Branch. These two quantities cannot generally be determined otherwise, except for some masses of sdB stars known through the study of binary systems containing an sdB component, but with a relatively poor accuracy on the derived value. For its part, the determination of the mass of the outer H-rich envelope is a pure product of asteroseismology and, beside theory, this quantity cannot be constrained by other known means. Determinations of $M_{\rm env}/M_*$ for other EC 14026 pulsators through our seismic approach may provide, in the future, an interesting insight into the internal structure and evolution of these extreme horizontal branch stars. Finally, we point out that our determination of the distance from Earth of Feige 48 is remarkably consistent with the distance of 755 ± 90 pc derived from independent methods by O'Toole et al. (2004).

As a concluding remark of this subsection, we mention that we are fully aware that our asteroseismic determinations of the global parameters of Feige 48 are only as good, in an absolute sense, as the constitutive physics that went into the construction of the equilibrium models. Future improvements in our ability to understand and model sdB stars at the level of the microphysics (i.e., the equation of state, the opacity, the radiative levitation, initial conditions, and so on) will necessarily lead to revised estimates of these parameters and, hopefully, to improved matches of the observed periods. Nevertheless, we think that solid credibility must already be given to current available constitutive physics since, after reproducing the 13 observed pulsation periods of PG 0014+067 to better than ∼0.8% Brassard et al. (2001) and the 9 observed periods of PG 1219+534 to better than ∼0.6% (Charpinet et al. 2005), the current models are also able to explain the presence of four independent pulsation periods in the star Feige 48, a rapid sdB pulsator with significantly different properties than the other EC 14026 stars analysed so far, with an average accuracy of ∼0.005% on the periods.

4.6. Feige 48 as a moderate rotator

As pointed out in Sect. 3, the existence of fine structure in the period spectrum of Feige 48 (see Table 2) is most simply interpreted as the signature of the relatively slow rotation of the star. As it is well known in stellar pulsation theory, rotation lifts the $2\ell + 1$ fold-degeneracy in frequency of a pulsation mode

defined by the doublet of indices (k, ℓ) in a perfectly spherical model. It thus produces $2\ell + 1$ components of different frequencies now specified by the triplet of indices (k, ℓ, m). It is likely that we have detected the strongest components of rotationally split multiplets. Treated as a first order perturbation and assuming solid body rotation (an assumption justified below), the net effect is having the modes with adjacent values of m (i.e., $|\Delta m| = 1$ with the same k and ℓ values) being evenly separated with a frequency spacing given by

$$\Delta\nu_{k\ell} = \frac{1 - C_{k\ell}}{P_{\rm rot}}, \quad (1)$$

where $\Delta\nu_{k\ell}$ is expressed in Hz, the rotation period $P_{\rm rot}$ is given in s, and $C_{k\ell}$ is the dimensionless first-order rotation coefficient encountered previously in our discussion of Table 3. Again, we point out that for p-modes and g-modes of degree $\ell \gtrsim 2$, this coefficient is usually very small compared to unity and therefore has little weight in Eq. (1).

All the multiplet components identified in the light curve of Feige 48 have an approximately (but not strictly) constant frequency spacing found in the range 25−31.2 μHz. Small variations in this frequency spacing may be due to different values of the $C_{k\ell}$ coefficients (as these slightly depend on the k and ℓ indices), to possible departure from the original assumption of solid rotation, and/or to small second-order effects caused by rotation. Nonetheless, an average frequency spacing derived from the available modes gives $\overline{\Delta\nu} \simeq 28.2$ μHz, with a standard deviation of $\sigma(\Delta\nu) \simeq 2.48$ μHz. Considering our resolution of 2.17 μHz which is of the same order as the standard deviation found for the frequency spacing, we find justified to use that average value to estimate the rotation period of Feige 48. Similarly, based on Table 3, we can compute an average value and standard deviation for the quantity $\overline{D} \equiv \overline{1 - C_{k\ell}}$, i.e., the numerator in the right-hand side of Eq. (1), leading to $\overline{D} = 0.958 \pm 0.036$. Using these average values in Eq. (1), we derive $P_{\rm rot} = 9.44 \pm 1.18$ hr. This value is consistent with the estimate for the rotation period of Feige 48 provided by Reed et al. (2004). If we now combine this result with our estimate of the radius of the star provided in Table 5, we find an equatorial velocity $V_{\rm eq} = 2\pi R/P_{\rm rot} = 27.6 \pm 3.9$ km s^{-1}. It is interesting to compare this value of the maximum broadening velocity with the results of Heber et al. (2000), who have set a limit of $V_{\rm eq} \sin i \lesssim 5$ km s^{-1}. Our evaluation of a relatively fast rotation rate based on the interpretation of rotationally induced mode splitting thus indicates that this star is most likely a moderate rotator seen nearly pole-on, with an inclination angle $i(^\circ) \lesssim 10.4 \pm 1.7$. Interestingly, in the recent discovery by O'Toole et al. (2004) that Feige 48 has a relatively close companion (likely a white dwarf), these authors found that the orbital period of the system is $P_{\rm orb} = 9.02 \pm 0.03$ h and they provided a limit for the inclination angle of the system which is $i(^\circ) \lesssim 11.4$. These values are remarkably consistent with our own evaluation derived from asteroseismology. In particular, we find that our estimate of the rotation period of Feige 48 falls very close to the measured orbital period. One would expect, indeed, such a relatively tight binary system to be phase locked due to tidal interaction, with both components rotating as solid bodies. This justifies a posteriori the assumption of solid rotation used to evaluate the rotation period of this star from the fine structure in its pulsation spectrum.

5. Summary and conclusion

We observed the luminosity variations of the relatively bright ($V = 13.46 \pm 0.02$), rapidly pulsating hot B subdwarf Feige 48 at high sensitivity at the CFHT in 1998, June. Such observations were part of an ongoing, long-term project to monitor the pulsations of EC 14026 stars at sufficiently high S/N ratios to allow for the detection of low-amplitude modes. The goal is to increase the number of detected modes in known EC 14026 stars, as it constitutes a necessary step for ultimately applying asteroseismic methods to probe the inner structure of these objects. For this purpose, the use of the Montréal 3-channel photometer LAPOUNE at the CFHT has proved to be particularly efficient. For all sdB pulsators observed so far in the course of this program, we could typically double the number of mode detections compared to existing data from other sites (see Charpinet 2001). This allowed for detailed asteroseismic analyses of several sdB stars, including PG 0014+067 (Brassard et al. 2001) and PG 1219+534 (Charpinet et al. 2005). The high sensitivity observations of Feige 48 reported in this paper provide a similar outcome with the clear identification of nine oscillation periods. This constitutes a significant improvement over the previous, lower S/N ratio data available for this star that allowed for the detection of only five periodicities (Koen et al. 1998; Reed et al. 2004).

From the time series analysis using standard methods that combine Fourier analysis, least squares fits of the light curve, and prewhitening methods, we found that Feige 48 has a relatively simple pulsation spectrum even when observed at high sensitivity. The period spectrum is most simply interpreted by assuming that the star oscillates in four independent modes that possess fine structure likely due to rotation. We find that the rotationally split components have an average frequency spacing of $\overline{\Delta\nu} \sim 28.2$ μHz. Assuming solid-body rotation, this frequency spacing indicates that Feige 48 rotates with a period of $P = 9.44 \pm 1.18$ h. O'Toole et al. (2004) have recently discovered that Feige 48 is the member of a relatively close binary system containing a white dwarf. They measured an orbital period of 9.02 ± 0.03 h for the system which is quite close to our derived rotation period. As one would expect for such a binary system, this result indicates that Feige 48 is very likely a solid-body rotator that is tidally locked to its companion.

Based on the four independent oscillation periods identified in the light curve of Feige 48, we have attempted a detailed asteroseismic analysis of this EC 14026 star. Our approach relied on the well-known forward method with the goal of finding objectively the model that would best match the set of periods observed in this star with a set of theoretical periods. We have used the second generation sdB models of Charpinet et al. (1997) to compute the theoretical periods since those have proved to account quite well for the class properties of the EC 14026 pulsators (Charpinet et al. 2001). These models are specified by four free parameters which are the surface gravity $\log g$, the effective temperature $T_{\rm eff}$, the stellar mass $M_*/M_\odot$, and the fractional mass of the hydrogen rich envelope $\log [M({\rm H})/M_*]$. Using the Toulouse package of numerical tools

that we have developed over the years for asteroseismology, we performed a double-optimisation procedure that takes place simultaneously at the period matching level and in the model parameter space (see Charpinet et al. 2005). However, due to the small number of independent modes available to constrain the models, we adopted the effective temperature measurement provided by spectroscopic means and limited the search in the three-dimensional space defined by the remaining free model parameters. An ongoing project aimed at improving the spectroscopic characterisation of sdB stars (including both the rapid and slow pulsators), and which is based on the acquisition of medium resolution, high S/N ratio spectra with the blue spectrograph at the new MMT, has proved essential in this context.

Our thorough exploration of the reduced three-dimensional parameter space led us to first isolate two families of model solutions that best-match the observed periods of Feige 48. These families of models have surface gravities around $\log g \sim 5.44$ and $\log g \sim 5.34$, respectively, and correspond to slightly different mode identifications. This degeneracy in the asteroseismic solution could be lifted solely on the basis of period fit quality, but other constraints confirmed also this choice. Such constraints were provided by the available spectroscopic measurements for the atmospheric parameters of Feige 48. Our estimate, $T_{\rm eff} = 29\,580 \pm 370$ K and $\log g = 5.480 \pm 0.046$, which is consistent with existing independent measurements from other groups, allowed us to confirm the family of model solutions found at higher surface gravity (i.e., near $\log g \sim 5.44$). Concentrating on this preferred solution, we found however that degeneracies still exist which preclude from uniquely isolating an optimal model from asteroseismology alone. This problem occurs due to concurrent effects of model parameters on the pulsation periods, leading to line degeneracies of the best-fit solutions. We found, for instance, that seismic solutions of comparable quality exist for all values of the total mass of the star, but these solutions have values for $T_{\rm eff}$ that are correlated. The trend uncovered is monotonic and indicates that optimal models of low-mass (down to 0.30 $M_{\odot}$) require cooler effective temperatures, while optimal models of high-mass (up to 0.70 $M_{\odot}$) need hotter effective temperatures. It is again spectroscopy that provided the additional information needed to bypass this difficulty. Using the well-constrained value of $T_{\rm eff}$ derived from this method led to the determination of a unique viable optimal model solution that fit consistently Feige 48, both asteroseismically and spectroscopically.

The basic properties of Feige 48 as inferred from our combined spectroscopic and asteroseismic approach have been summarised in Table 5. The quest for an optimal seismic model of Feige 48 has revealed that accurate spectroscopy remains an essential ingredient for detailed asteroseismology of EC 14026 stars in order to converge toward a unique solution. A relatively precise determination of the surface gravity using spectroscopic techniques is generally helpful to discriminate between families of potential seismic solutions. Once the "right" family has been chosen, though, the constraint brought by asteroseismology on the value of $\log g$ is much tighter than the precision that spectroscopy can currently provide. This is one of the outstanding outcome of asteroseismology as it leads to measurements of the surface gravity of EC 14026 stars at unprecedented accuracy (a gain in accuracy of a factor ~10, typically). The opposite is true for the effective temperature and the spectroscopic value for this parameter must clearly be preferred. Moreover, in the case of Feige 48, the line degeneracy uncovered for the seismic solution precludes from having an independent measurement of $T_{\rm eff}$ through asteroseismological means.

Another outcome of asteroseismology is the measurement of the total mass and the mass of the H-rich envelope at an interesting level of accuracy. In our study of Feige 48, we found however that these quantities could not be inferred independently of the spectroscopic measurement of the effective temperature. Nonetheless, the value derived for the total mass, $M = 0.460 \pm 0.008\ M_{\odot}$, indicates a mass of Feige 48 that is close to the canonical value commonly admitted for sdB stars. Although this value of the mass depends on how reliable the spectroscopic estimate of $T_{\rm eff}$ is (particularly in regards of eventual systematic effects), we stress that significantly different masses than the derived – close to canonical – value, such as some scenarios of binary evolution suggest, would require a shift of several thousand Kelvins in effective temperature to be compatible with asteroseismology. Such a drastic change in the evaluation of $T_{\rm eff}$ from spectroscopy is highly unlikely and, therefore, we are confident in concluding that Feige 48 has a mass close to the canonical mass of extreme horizontal branch stars. Notably, we also found that Feige 48 has a somewhat thicker hydrogen-rich envelope mass, with $\log (M_{\rm env}/M_{*}) = -2.97 \pm 0.09$, than the other significantly hotter and more compact sdB pulsators probed so far by asteroseismology, namely PG 0014+067 having $\log (M_{\rm env}/M_{*}) = -4.31 \pm 0.22$ (Brassard et al. 2001), and PG 1219+534 with $\log (M_{\rm env}/M_{*}) = -4.25 \pm 0.15$ (Charpinet et al. 2005). This result is interesting in that it follows – and hence, for the first time, directly confirms – the current wisdom from standard evolution theory that EHB stars with cooler effective temperatures and lower surface gravities have thicker H-rich envelopes.

Finally, we found that our optimal model solution is able to reproduce simultaneously the four independent periods observed in Feige 48 with an unprecedented average dispersion of only ~0.005%. The observed periods correspond to low-order $\ell = 0$, 1, and 2 modes that are, indeed, predicted to be excited according to nonadiabatic pulsation theory. It is a remarkable result that a model solution exist for Feige 48 which can, at the same time, reproduce all the periods observed in this star at a very high level of accuracy, be consistent with nonadiabatic theory, and satisfy the spectroscopic constraints. Such a consistency between three independent aspects of the modelling of these pulsating stars is a result that was not guaranteed at the outset. This is a strong indication that the basic constitutive physics which enters in the construction of our current models used for the asteroseismic analyses of EC 14026 stars is sound, especially as it follows similar results already obtained for the rapid sdB pulsators PG 0014+067 and PG 1219+534 (Brassard et al. 2001; Charpinet et al. 2005). Furthermore, the excellent agreement between observations and theory at the nonadiabatic level again confirms that the iron bump opacity mechanism of Charpinet et al. (1997) is at the origin of the EC 14026 phenomenon.

Acknowledgements. This work was supported in part by the NSERC of Canada and by the Fund FQRNT (Québec). G.F. also acknowledges the contribution of the Canada Research Chair Program.

References

Billères, M., Fontaine, G., Brassard, P., et al. 1997, ApJ, 487, L81
Billères, M., Fontaine, G., Brassard, P., & Liebert, J. 2002, ApJ, 578, 515
Brassard, P., & Fontaine, G. 1994, in The Equation of State in Astrophysics, IAU Coll., 147, 560
Brassard, P., Pelletier, C., Fontaine, G., & Wesemael, F. 1992, ApJS, 80, 725
Brassard, P., Fontaine, G., Billères, M., et al. 2001, ApJ, 563, 1013
Charpinet, S. 2001, Astron. Nachr., 322, 387
Charpinet, S., Fontaine, G., Brassard, P., & Dorman, B. 1996, ApJ, 471, L103
Charpinet, S., Fontaine, G., Brassard, P., et al. 1997, ApJ, 483, L123
Charpinet, S., Fontaine, G., Brassard, P., & Dorman, B. 2000, ApJS, 131, 223
Charpinet, S., Fontaine, G., & Brassard, P. 2001, PASP, 113, 775
Charpinet, S., Fontaine, G., Brassard, P., & Dorman, B. 2002a, ApJS, 139, 487
Charpinet, S., Fontaine, G., Brassard, P., & Dorman, B. 2002b, ApJS, 140, 469
Charpinet, S., Fontaine, G., & Brassard, P. 2003, in White Dwarfs, NATO ASIB Proc., 105, 69
Charpinet, S., Brassard, P., & Fontaine, G. 2004, Ap&SS, 291, 395
Charpinet, S., Fontaine, G., Brassard, P., Green, E. M., & Chayer, P. 2005, A&A, 437, 575
D'Cruz, N. L., Dorman, B., Rood, R. T., & O'Connell, R. W. 1996, ApJ, 466, 359
Dorman, B., Rood, R. T., & O'Connell, R. W. 1993, ApJ, 419, 596
Feige, J. 1958, ApJ, 128, 267
Fontaine, G., Brassard, P., Wesemael, F., & Tassoul, M. 1994, ApJ, 428, L61
Fontaine, G., Brassard, P., Charpinet, S., et al. 2003, ApJ, 597, 518
Graham, J. A. 1970, PASP, 82, 1305
Green, E. M., Fontaine, G., Reed, M. D., et al. 2003, ApJ, 583, L31
Han, Z., Podsiadlowski, P., Maxted, P. F. L., Marsh, T. R., & Ivanova, N. 2002, MNRAS, 336, 449
Han, Z., Podsiadlowski, P., Maxted, P. F. L., & Marsh, T. R. 2003, MNRAS, 341, 669
Heber, U. 1986, A&A, 155, 33
Heber, U., Reid, I. N., & Werner, K. 2000, A&A, 363, 198
Jeffery, C. S., Dhillon, V. S., Marsh, T. R., & Ramachandran, B. 2004, MNRAS, 352, 699
Kilkenny, D. 2002, in Radial and Nonradial Pulsationsn as Probes of Stellar Physics, ASP Conf. Ser., 259, IAU Coll., 185, 356
Kilkenny, D., Koen, C., O'Donoghue, D., & Stobie, R. S. 1997, MNRAS, 285, 640
Koen, C., O'Donoghue, D., Pollacco, D. L., & Nitta, A. 1998, MNRAS, 300, 1105
O'Toole, S. J., Heber, U., & Benjamin, R. A. 2004, A&A, 422, 1053
Reed, M. D., Kawaler, S. D., Zola, S., et al. 2004, MNRAS, 348, 1164
Saffer, R. A., Bergeron, P., Koester, D., & Liebert, J. 1994, ApJ, 432, 351
Silvotti, R., Østensen, R., Heber, U., et al. 2002, A&A, 383, 239
Stobie, R. S., Kawaler, S. D., Kilkenny, D., O'Donoghue, D., & Koen, C. 1997, MNRAS, 285, 651
Wesemael, F., Fontaine, G., Bergeron, P., Lamontagne, R., & Green, R. F. 1992, AJ, 104, 203